PAPER

Short-range forces due to Lorentz-symmetry violation

To cite this article: Quentin G Bailey et al 2023 Class. Quantum Grav. 40 045006

View the article online for updates and enhancements.

You may also like

- <u>Discrete Lorentz symmetry and discrete</u> time translational symmetry Pei Wang
- What do we know about Lorentz invariance? Jay D Tasson
- Abelian geometric phase for a Dirac neutral particle in a Lorentz symmetry violation environment K Bakke and H Belich

Short-range forces due to Lorentz-symmetry violation

Quentin G Bailey^{1,*}, Jennifer L James², Janessa R Slone¹ and Kellie O'Neal-Ault¹

- ¹ Embry-Riddle Aeronautical University, 3700 Willow Creek Road, Prescott, AZ 86301, United States of America
- ² Vanderbilt University, 2201 West End Avenue, Nashville, TN 37235, United States of America

E-mail: baileyq@erau.edu

Received 13 October 2022; revised 8 December 2022 Accepted for publication 5 January 2023 Published 23 January 2023



Abstract

Complementing previous theoretical and experimental work, we explore new types of short-range modifications to Newtonian gravity arising from spacetime-symmetry breaking. The first non-perturbative, i.e. to all orders in coefficients for Lorentz-symmetry breaking, are constructed in the Newtonian limit. We make use of the generic symmetry-breaking terms modifying the gravity sector and examine the isotropic coefficient limit. The results show new kinds of force law corrections, going beyond the standard Yukawa parameterization. Further, there are ranges of the values of the coefficients that could make the resulting forces large compared to the Newtonian prediction at short distances. Experimental signals are discussed for typical test mass arrangements.

Keywords: Lorentz symmetry, short-range forces, tests of general relativity, spacetime symmetry tests

(Some figures may appear in colour only in the online journal)

1. Introduction

Presently, the nature of gravity is still largely unknown on length scales less than micrometers. In fact, new types of forces many times stronger than the Newtonian gravitational force could exist on short length scales and still be consistent with current experimental limits [1]. Suggestions for hypothetical new forces that could modify gravity at short ranges abound in the literature [2–8]. In particular, miniscule but potentially detectable violations of fundamental

1361-6382/23/045006+29\$33.00 © 2023 IOP Publishing Ltd Printed in the UK

^{*} Author to whom any correspondence should be addressed.

symmetries underlying general relativity (GR) can arise in a plethora of ways [9–15]. The breaking of local Lorentz symmetry, for instance, can modify gravity on short ranges while being consistent with longer range measurements [16, 17].

To categorize the phenomenology of spacetime symmetry breaking one needs a comprehensive test framework. Effective field theory (EFT) is a widely used tool for describing potentially detectable new physics [18]. EFT descriptions of spacetime-symmetry breaking, including local Lorentz symmetry breaking, are based on including the action of GR and a standard matter sector action [19]. To these basic pieces, are added a series of symmetry breaking terms that can be organized by number of derivatives, curvature, mass dimensions, and so on [20–22]. This approach has the advantage that one can in principle calculate the effect on some observable due to some symmetry breaking terms, which can then be compared with entirely different observables in different scenarios, for measurements of the same coefficients controlling the size of the effects. Other formalisms for testing symmetries in gravity are parametrized directly from the form of a GR observable [23–25], or are based on specific models of alternatives to GR [26–29].

We will consider in this work modifications to the gravity sector that, contrary to standard GR, break local Lorentz symmetry and diffeomorphism symmetry explicitly or spontaneously. These spacetime symmetries can be thought of as gauge symmetries for gravity, and thus GR is a gauge theory of gravity with local Lorentz and diffeomorphism symmetries as the gauge symmetries, analogous to Standard Model physics based on gauge groups [30]. The subtle issue of the role of broken spacetime symmetries in the context of curved spacetime, particularly when assuming asymptotically flat scenarios or not, has been discussed at length elsewhere [22, 31, 32]. While we do not fully discuss these concepts and subtleties here, we shall refer to conventions and categories of transformations in these references as needed.

In the EFT approach taken here, we highlight comparison of short-range (SR) gravity tests with gravitational wave (GW) observations, thus comparing two tests 'across the Universe' for measuring the same quantities describing spacetime-symmetry breaking for gravity. In fact, we show certain rotational scalar coefficients that can be measured in GW tests can also be probed in SR tests. Further, there are some coefficients that cannot be completely disentangled with GW tests alone, but using also SR gravity tests could accomplish this.

In [16, 17] solutions for SR gravity tests were found, but these used an approximation of leading order in the coefficients. We show here that exact, non-perturbative, solutions can reveal where other combinations of coefficients, not yet disentangled, can show up in experiment. As we are concerned in this paper with modifications to gravity that do not break the Weak-Equivalence Principle, we do not discuss WEP violations here. The connection between Lorentz violation and WEP has been discussed at length elsewhere [33–36].

Since we examine non-perturbative solutions, the results in this work also touch on the nature of higher than second order derivatives in the action and how that might affect gravity. For this latter topic, we do not attempt a comprehensive investigation of these issues but simply note where results exhibit behavior expected of such models [37–39], and how they might be consistent with perturbative approaches.

The paper is organized as follows. In section 2, we review two commonly used EFT schemes for the description of spacetime symmetry breaking in gravity and we discuss prior results in SR gravity signals for Lorentz violation. In section 3, we explore non-perturbative solutions with a special case model to identify key features. Following this, we go on to solve the general EFT framework in the static, isotropic coefficient limit. Features of the solutions are discussed and explained with several plots. We discuss attempting exact solutions with anistropic coefficients in section 4, and compare to perturbative methods. For section 5, we apply the theoretical results to simulate the signal of the gravitational field above a flat plate of mass, and comment

on the experimental signatures. A summary and outlook is provided in section 6. Finally, in the appendix we include a review of relevant differential equations, the details of the tensor analysis for isotropic coefficients used, and special cases of the SR gravity solutions. In this work, we assume four-dimensional spacetime with metric signature -+++ and units where $\hbar=c=1$. Latin letters are used for three-dimensional space, and Greek letters for spacetime indices.

2. Background theory

2.1. Action and field equations

One can work with an observer covariant EFT expansion or an action designed for weak-field applications, the latter formulated in a quadratic action expansion. The two approaches are overlapping descriptions of physics beyond GR and the SM when spacetime symmetries are broken. We display both approaches here, to emphasize recent points of view in the literature, and because we use them in this work.

It is a basic premise that in the EFT context, a breaking of spacetime symmetries is indicated by the presence of a background tensor field of some kind that couples to matter or gravity or both [9, 19, 20]. The details and subtleties of this premise have been discussed at length elsewhere [22, 31, 32]. Suffice it to say here that the EFT maintains coordinate invariance of physics (observer invariance) while the action may not be invariant under symmetry transformations of localized field configurations (particle transformations). The latter violation is due to the presence of the background tensor fields, which remain fixed under such transformations.

The observer covariant expansion has a Lagrange density that takes the form of a series of terms:

$$\mathcal{L} = \frac{\sqrt{-g}}{2\kappa} \left(R + k_{\alpha\beta\gamma\delta}^{(4)} R^{\alpha\beta\gamma\delta} + k_{\alpha\beta\gamma\delta\kappa}^{(5)} \nabla^{\kappa} R^{\alpha\beta\gamma\delta} + k_{\kappa\lambda\mu\nu\alpha\beta\gamma\delta}^{(6)} R^{\kappa\lambda\mu\nu} R^{\alpha\beta\gamma\delta} + \cdots \right) + \mathcal{L}'.$$
(1)

In this expression, the determinant of the metric is $\sqrt{-g}$, $R^{\alpha\beta\gamma\delta}$ is the Riemann curvature tensor, R is the Ricci scalar, and $k_{\alpha\beta\gamma\delta}^{(4)}$, $k_{\alpha\beta\gamma\delta\kappa}^{(5)}$, and $k_{\kappa\lambda\mu\nu\alpha\beta\gamma\delta}^{(6)}$ are the coefficients controlling the degree of symmetry breaking [16, 22]. The coupling is $\kappa=8\pi G_N$, where G_N is the gravitational constant. The first term is the Einstein–Hilbert lagrange density, while the remaining terms are the symmetry-breaking terms. Note that additional terms for the coefficients can be included in \mathcal{L}' . For instance, a general expansion for such terms exists, for the case of a two-tensor $s_{\mu\nu} \propto k_{\mu\alpha\nu}^{(4)\alpha}$, and takes the form

$$\mathcal{L}' = \frac{\sqrt{-g}}{2\kappa} \left[a_3 \frac{1}{2} (\nabla_{\mu} s_{\nu\lambda}) (\nabla^{\mu} s^{\nu\lambda}) + a_4 \frac{1}{2} (\nabla_{\mu} s^{\mu\lambda}) (\nabla_{\lambda} s_{\beta}^{\beta}) + \dots + a_7 s_{\mu\nu} s_{\kappa\lambda} R^{\mu\kappa\nu\lambda} + a_8 s_{\mu\nu} s_{\lambda}^{\mu} R^{\nu\lambda} + \dots \right], \tag{2}$$

which can be viewed as terms of second order in the coefficients or as dynamical terms [32, 40]. Alternatives to (2) can adopt the explicit symmetry breaking scenario, where the coefficients in (1) are given *a priori*, this latter possibility given emphasis more recently [41–44].

An alternative overlapping approach, the quadratic action approach, assumes an expansion around flat spacetime $\eta_{\mu\nu}$, of the standard form

$$g_{\mu\nu} = \eta_{\mu\nu} + h_{\mu\nu}.\tag{3}$$

We examine the quadratic action [45, 46] in the limit that maintains the usual linearized gauge invariance of GR: $h_{\mu\nu} \to h_{\mu\nu} - \partial_{\mu}\xi_{\nu} - \partial_{\nu}\xi_{\mu}$. The Lagrange density for this approach takes the form

$$\mathcal{L} = -\frac{1}{4\kappa} h^{\alpha\beta} G_{\alpha\beta} + \frac{1}{8\kappa} h_{\mu\nu} (\hat{s}^{\mu\rho\nu\sigma} + \hat{q}^{\mu\rho\nu\sigma} + \hat{k}^{\mu\rho\nu\sigma}) h_{\rho\sigma}, \tag{4}$$

where $G_{\alpha\beta}$ is the linearized Einstein tensor. The 'hat' operators are built from background coefficients for spacetime-symmetry breaking and partial derivatives. The three types appearing in (4) are given by,

$$\hat{s}^{\mu\rho\nu\sigma} = s^{(d)\mu\rho\epsilon_{1}\nu\sigma\epsilon_{2}...\epsilon_{d-2}} \partial_{\epsilon_{1}}...\partial_{\epsilon_{d-2}},$$

$$\hat{q}^{\mu\rho\nu\sigma} = q^{(d)\mu\rho\epsilon_{1}\nu\epsilon_{2}\sigma\epsilon_{3}...\epsilon_{d-2}} \partial_{\epsilon_{1}}...\partial_{\epsilon_{d-2}},$$

$$\hat{k}^{\mu\nu\rho\sigma} = k^{(d)\mu\epsilon_{1}\nu\epsilon_{2}\rho\epsilon_{3}\sigma\epsilon_{4}...\epsilon_{d-2}} \partial_{\epsilon_{1}}...\partial_{\epsilon_{d-2}}.$$
(5)

While the expansions in (5) appear similar for the three types of coefficients, the s, q, and k in fact differ by symmetry and tensor properties. The detailed tensor properties of these terms are described in the Young tableau of table 1 of [45], (some samples are included in appendix (59)). In particular, $\hat{s}^{\mu\rho\nu\sigma}$ is anti-symmetric in the pairs of indices $\mu\rho$ and $\nu\sigma$, while $\hat{q}^{\mu\rho\nu\sigma}$ is anti-symmetric in $\mu\rho$ and symmetric in $\nu\sigma$, and finally $\hat{k}^{\mu\nu\rho\sigma}$ is symmetric in the pairs of indices $\mu\rho$ and $\nu\sigma$. In terms of discrete spacetime symmetries, The \hat{s} operators have even CPT symmetry and mass dimension $d \geqslant 4$; \hat{q} operators have odd CPT and mass dimension $d \geqslant 5$; \hat{k} operators have even CPT and mass dimension $d \geqslant 6$.

The phenomenology of the terms in (1) and (4) has been studied in a number of works. Observable effects in weak-field gravity tests have been established for a subset of the possible terms [16, 47, 48] and some work has been done on strong-field gravity regimes like cosmology [42, 49–51]. Effects on GWs have been studied, showing that dispersion and birefringence occur generically as a result of CPT and Lorentz violation [45]. Analysis has been performed in tests such as lunar laser ranging [52], gravimetry [53], pulsars [54], and using the catalog of GW events [55–59]. An exhaustive list of up to date experimental limits and papers on gravity sector coefficients can be found in [60].

On the theory side, explicit local Lorentz and diffeomorphism symmetry cases have been explored various contexts. A '3+1' formulation of the EFT framework has been explored in [42, 43, 61]. Extensive work has been completed mapping out the approach to explicit symmetry breaking with Finsler geometry [62–65]. Other work includes much attention to vector and tensor models of spontaneous symmetry breaking [26, 27, 66–70] and how these models can be matched to the EFT expansion above [42, 44, 71, 72]. More recently, black hole solutions have been studied [73–75]. Also, the systematic construction of dynamical terms for the spontaneous symmetry breaking scenario, like in (2), has been undertaken in the gravity sector [40]. Finally we note some recent theoretical work has identified general properties of backgrounds in EFT [32], and new types of tests are possible that search for non-Riemann geometry [76].

Of the two approaches identified above, the latter, equation (4), is appropriate for SR gravity tests. Such tests involve weak gravitational fields in the Earth laboratory setting, thus the typical size of components of $h_{\mu\nu}$ are much less than unity, in cartesian coordinates. Furthermore, to keep a reasonable scope we will truncate the series (5) to mass dimensions 4, 5, and 6.

Any study of actions with higher than second order derivatives is subject to well-known results, such as Ostragradsky instabilities [39]. In the present paper, while the test framework (4) is viewed perturbatively, with the higher derivative terms as small corrections [77], our discussion of solutions beyond leading order in coefficients will overlap with features in higher derivative models. Some features are discussed in our results in sections 3 and 4.

2.2. Prior SR gravity results

In [16, 17], Lorentz-symmetry breaking solutions for SR gravity tests were found using an approximation of first order in the coefficients. We summarize these results briefly here for comparison. Assuming a static matter source and using the framework of (4), one solves the field equations perturbatively assuming any modifications to the field equations from symmetry-breaking terms are small [16, 17, 47]. The leading order modified Newtonian potential from a point mass m at the origin can be written in terms of Newton spherical coefficients $k_{im}^{N(d)lab}$ as a series

$$U = \frac{G_N m}{r} + \sum_{djm} \frac{G_N m}{r^{d-3}} Y_{jm}(\theta, \phi) k_{jm}^{N(d)lab}, \tag{6}$$

where the angular dependence θ , ϕ in the spherical harmomics $Y_{jm}(\theta,\phi)$ pertains to the vector from the origin to the field point $\vec{r} = r(\sin\theta\cos\phi,\sin\theta\sin\phi,\cos\theta)$ and $r = |\vec{r}|$. The spherical coefficients $k_{jm}^{N(d)lab}$ are related to the coefficients in equation (5) as linear combinations, but the expressions are lengthy and omitted here, and relations between the dimension label (*d*) and the allowed values of *j* can be found in [17]. The superscript 'lab' means that the coefficients are written in the laboratory coordinate system. Typically, the lab frame coefficients are re-expressed in terms of the Sun-centered Celestial Equatorial Frame coefficients using an observer Lorentz transformation, revealing harmonic time dependence [78–80].

The result in equation (6) has already been used for analysis in experiments [81–84]. In fact, new experiments can be designed to maximize the type of anisotropic signal in (6) [83, 85, 86]. Recent result place limits on $14 k_{jm}^{N(6)}$ coefficients and $22 k_{jm}^{N(8)}$ coefficients at the $10^{-9} m^2$ and $10^{-12} m^4$ levels, respectively. However, the leading order approximation used for (6) makes searches in some SR tests challenging, as some tests are designed to probe very small length scales at the cost of sensitivity to the Newtonian force from the test masses [87]. Such tests often lie outside the range of applicability of the result (6), which assumes the extra correction term to the Newtonian potential is smaller than the first term.

One other observation is that, with the exception of mass dimension four coefficients, no rotational scalar coefficients, or isotropic coefficients show up in the result (6). In fact, it has been shown that one combination of isotropic coefficients does show up in the perturbative analysis, but only as contact term that vanishes outside of the matter distribution [16]. As we show below, a non-perturbative treatment reveals in more detail the role played by these coefficients.

3. Isotropic coefficients, Newtonian limit, nonperturbative

3.1. Special case model

We begin with a special case to illustrate the features of the solutions studied in this work. One particular model that contains the interesting features of exact SR solutions is the following Lagrange density:

$$\mathcal{L} = \frac{1}{2\kappa} \sqrt{-g} \left(R + k_{\alpha\beta} R^{\alpha\beta} R \right), \tag{7}$$

which is a special case of (1). The second term is the non-standard one with the coefficients for Lorentz violation denoted $k_{\alpha\beta}$. These ten quantities have units of length squared or inverse mass squared in natural units.

The action in (7), yields the field equations in appendix (53), upon variation with respect to the full metric $g_{\mu\nu}$. In the linearized gravity limit, and assuming the coefficients $k_{\alpha\beta}$ have vanishing partials $\partial_{\alpha}k_{\beta\gamma}=0$, the field equation (53) become,

$$(G_L)^{\mu\nu} = -\frac{1}{2}\eta^{\mu\nu}k_{\alpha\beta}\partial^{\alpha}\partial^{\beta}R_L - \eta^{\mu\nu}k_{\alpha\beta}\partial^{\gamma}\partial_{\gamma}(R_L)^{\alpha\beta} + \frac{1}{2}k^{\nu\alpha}\partial_{\alpha}\partial^{\mu}R_L + \frac{1}{2}k^{\mu\alpha}\partial_{\alpha}\partial^{\nu}R_L + k_{\alpha\beta}\partial^{\mu}\partial^{\nu}(R_L)^{\alpha\beta} - \frac{1}{2}k^{\mu\nu}\partial^{\alpha}\partial_{\alpha}R_L + \kappa T^{\mu\nu},$$
(8)

where $T^{\mu\nu}$ is the matter stress-energy tensor. Note that in the linearized gravity case, indices are raised and lowered with $\eta_{\mu\nu}$, the linearized Ricci tensor is $(R_L)_{\mu\nu} = (1/2)(\partial_\mu \partial^\alpha h_{\alpha\nu} + \partial_\nu \partial^\alpha h_{\alpha\mu} - \partial_\alpha \partial^\alpha h_{\mu\nu} - \partial_\mu \partial_\nu h_\alpha^\alpha)$, $R_L = \partial^\alpha \partial^\beta h_{\alpha\beta} - \partial_\alpha \partial^\alpha h_\beta^\beta$, and $(G_L)^{\mu\nu} = (R_L)^{\mu\nu} - (1/2)\eta^{\mu\nu}R_L$. The task is next to obtain a space and time component decomposition of these field equation (8).

If we further restrict attention to the static limit and only isotropic coefficients k_{00} and k_{jj} , in a special coordinate system, we obtain the following coupled equations for the metric components h_{00} and h_{jj} (in harmonic gauge):

$$\nabla^{2}(h_{00} + h_{jj}) - 3(k_{00} - \frac{1}{9}k_{ll})\nabla^{4}h_{00} + (k_{00} - k_{ll})\nabla^{4}h_{jj} = -32\pi G_{N}\rho,$$

$$\nabla^{2}(3h_{00} + h_{jj}) + 4(k_{00} - \frac{1}{3}k_{ll})\nabla^{4}h_{00} + \frac{8}{3}k_{ll}\nabla^{4}h_{jj} = 0.$$
(9)

Note that $k_{ll} - k_{00} = k_{\mu\nu}\eta^{\mu\nu}$ is a Lorentz invariant scalar combination. We have assumed a static pressure-less matter distribution so that only $T^{00} = \rho$ is nonzero in $T^{\mu\nu}$. We also find in this limit that the equation for h_{0i} is simply Laplace's equation:

$$\nabla^2 h_{0i} = 0. \tag{10}$$

For the remaining components of h_{ij} it is advantageous to express the solution in terms of a traceless piece. By this we mean that if the equations for h_{ij} are denoted $\mathcal{E}_{ij} = 0$, the relevant projection is $\mathcal{E}_{ij} - (1/3)\delta_{ij}\mathcal{E}_{kk}$. This yields

$$\nabla^2 (h_{ij} - \frac{1}{3}\delta_{ij}h_{kk}) - 2(k_{00} - \frac{1}{3}k_{ll})\mathcal{D}_{ij}\nabla^2 h_{00} - \frac{4}{3}k_{ll}\mathcal{D}_{ij}\nabla^2 h_{kk} = 0, \tag{11}$$

where $\mathcal{D}_{ij} = \partial_i \partial_j - \frac{1}{3} \delta_{ij} \nabla^2$ is a traceless operator. Evidently, if one can solve independently for h_{00} and h_{II} , then equation (11) can be viewed as an inhomogeneous equation for the traceless piece of h_{ij} with source terms involving projections of h_{00} and h_{II} .

Our main focus is to solve the equations (9) for h_{00} and h_{jj} , since h_{00} is the metric component directly related to the Newtonian potential U_N via $h_{00} = 2U_N$. The solution can be found using standard methods of solving PDEs. We first discuss the construction of a Green function solution where we assume a point source $4\pi G_N \rho = \delta^{(3)}(\vec{r} - \vec{r}')$. The point source solutions for h_{00} and h_{jj} are denoted \mathcal{G}_1 and \mathcal{G}_2 .

Given the form of the solution to the equation with ∇^2 and ∇^4 in appendix (57), we propose the ansatz that the general solutions will take the form of the following functions of $R = |\vec{r} - \vec{r}'|$:

$$G_{1} = \frac{1}{R} \left(A_{1} e^{-q_{1}R} + A_{2} e^{-q_{2}R} + A_{3} \right),$$

$$G_{2} = \frac{1}{R} \left(B_{1} e^{-q_{1}R} + B_{2} e^{-q_{2}R} + B_{3} \right).$$
(12)

Here the A_n 's and B_n 's are constants to be solved for as well as the q_1 and q_2 . In constructing this solution we are assuming the boundary conditions such that the metric components go to zero far from the source, and we neglect any homogeneous solutions to (9). Insertion of (12) into the point source version of (9), followed by using the properties of functions of $R = |\vec{r} - \vec{r}'|$, allows one to solve for the eight parameters A_1 , A_2 , A_3 , B_1 , B_2 , B_3 , q_1 , and q_2 from eight resulting algebraic equations.

First, we find that for nontrivial solutions, both q_1^2 and q_2^2 must satisfy the quartic equation:

$$1 + (k_{00} - \frac{5}{3}k_{ll})q^2 + (k_{00} + \frac{1}{3}k_{ll})^2 q^4 = 0.$$
(13)

The solutions to (13) can be obtained from the quadratic result,

$$q^2 = u \pm v, (14)$$

where u and v are given by:

$$u = \frac{-(k_{00} - \frac{5}{3}k_{ll})}{2(k_{00} + \frac{1}{3}k_{ll})^{2}},$$

$$v = \frac{\sqrt{(k_{00} - \frac{5}{3}k_{ll})^{2} - 4(k_{00} + \frac{1}{3}k_{ll})^{2}}}{2(k_{00} + \frac{1}{3}k_{ll})^{2}}.$$
(15)

The four possible roots of the equation (13) can be obtained generally by taking the complex square roots of (14). The position of $z=q^2$ in the complex plane depends on the values of the coefficients k_{00} and k_{ll} . Note that u is real and v can be real or complex. The values of the coefficients determine the properties of the four possible roots $\{q=z^{1/2}=\pm(u\pm v)^{1/2}\}$. If q is entirely real and positive, then the solutions in (12) will exhibit exponential damping in R or SR Yukawa-like behavior. The case where q is negative and real will result in runaway exponential increase and is not physically viable. When q has an imaginary piece or is entirely imaginary, the solution will have oscillations in R.

In what follows we assume the condition $q_1^2 \neq q_2^2$. This condition ensures that the coefficients k_{00} and k_{ll} are treated *a priori* independent. This condition implies that in (14), q_1^2 takes one sign in the \pm , and q_2^2 takes the other sign. For this case we obtain the solutions for the Green function \mathcal{G}_1 as follows.

$$G_{1} = \frac{1}{2\pi R} - \frac{1}{4\pi} \left(1 + \frac{k_{00} + \frac{11}{3}k_{ll}}{\sqrt{(k_{00} - \frac{5}{3}k_{ll})^{2} - 4(k_{00} + \frac{1}{3}k_{ll})^{2}}} \right) \frac{e^{-R/\lambda_{+}}}{R} - \frac{1}{4\pi} \left(1 - \frac{k_{00} + \frac{11}{3}k_{ll}}{\sqrt{(k_{00} - \frac{5}{3}k_{ll})^{2} - 4(k_{00} + \frac{1}{3}k_{ll})^{2}}} \right) \frac{e^{-R/\lambda_{-}}}{R},$$
(16)

where the λ_{\pm} constants are defined by

$$\frac{1}{(\lambda_{\pm})^2} = u \pm v,\tag{17}$$

and they act like two distinct length scales.

We note the contrast of this result with previous results. First, unlike the Yukawa potential,

$$U_Y = \frac{Gm}{r} \left(1 + \alpha e^{-r/\lambda} \right),\tag{18}$$

we have two length scales in (17). Second, the amplitudes of the two terms vary depending on the values of the coefficients. In particular, we find that these amplitudes could take on large values for a narrow range of coefficient ratios k_{ll}/k_{00} , even if the coefficients themselves are small compared to the length scales probed. This is in contrast to standard assumptions of the smallness of Lorentz-violating effects. Note that the length scales would also be small, so such large Lorentz-breaking forces could escape detection in long-range tests, and this philosophy is along the lines of proposals for new SR forces more generally.

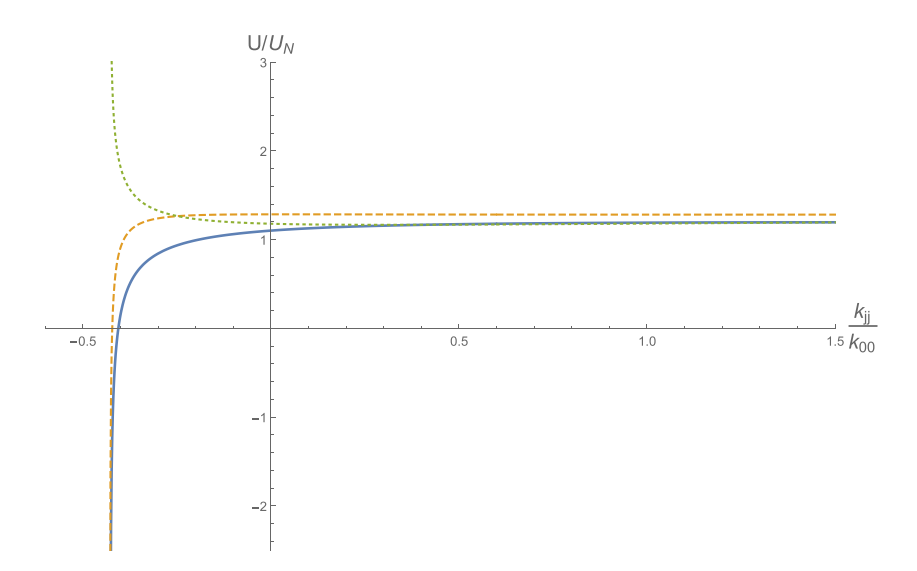


Figure 1. A plot of the ratio of the modified potential of equation (16) divided by the Newtonian potential for a unit mass at the origin. The horizontal axis is the coefficient ratio k_{jj}/k_{00} while the solid curve, dashed curve, and dotted curves are the cases of different positions away from the point mass, $R = \sqrt{k_{00}}$, $R = 3\sqrt{k_{00}}$, and $R = 5\sqrt{k_{00}}$, respectively.

To get an idea of the behavior of these solutions as the values of the coefficients change, in figure 1, we plot the potential $U=2\mathcal{G}_1$ for a point mass of unit strength as a function of k_{ll}/k_{00} for several values of the distance R (more specifically, the ratio of the distance R to $\sqrt{k_{00}}$). This can be compared to the standard Newtonian potential which would be a horizontal line in the same graph. We clearly see a singular point in the k_{ll} , k_{00} parameter space as the k_{ll}/k_{00} approaches -3/7.

The solution obtained in (16) above agrees precisely with an alternative method, where one uses Fourier decomposition in momentum space, followed by contour integration. For practical evaluation over distributions of matter, such as those used in experiment, one would take the integral of the Green functions over the smooth matter distributions $\rho(\vec{r}')$ as usual. Thus, since $h_{00} = 2U$, the Newtonian potential is

$$U = 2\pi G_N \int d^3r' \rho(\vec{r}') \mathcal{G}_1(\vec{r}, \vec{r}'). \tag{19}$$

3.2. General EFT case

Here we consider generalizing the solution of section 3.1. A more general treatment includes the quadratic Lagrange density of (4). First we examine the field equations for this approach, which are obtained from (4) by variation with respect to $h_{\mu\nu}$:

$$(G_L)^{\mu\nu} + \delta M^{\mu\nu\rho\sigma} h_{\rho\sigma} = 8\pi G_N T^{\mu\nu}, \tag{20}$$

where we have adopted the notation of [17] with

$$\delta M^{\mu\nu\rho\sigma} h_{\rho\sigma} = -\left[\frac{1}{4}(\hat{s}^{\mu\rho\nu\sigma} + \hat{s}^{\mu\sigma\nu\rho}) + \frac{1}{2}\hat{k}^{\mu\nu\rho\sigma} + \hat{q}^{\mu\rho\nu\sigma} + \hat{q}^{\mu\rho\nu\sigma} + \hat{q}^{\mu\sigma\nu\rho} + \hat{q}^{\nu\sigma\mu\rho}\right] h_{\rho\sigma}. \tag{21}$$

3.2.1. Determining the field equations. Next we will focus attention on mass dimension d=6 or less to keep the scope reasonable. Furthermore, as we are taking the static limit, as the prior section, only spatial derivatives appear. We will again choose to look at only isotropic coefficients, as these we expect to result in field equations we can solve exactly in analytic form, and to reveal the role of these coefficients in SR gravity tests.

It is not exactly trivial to extract the isotropic coefficients in the expansions (5) but we outline the process here and leave most of the details for the appendix. Consider the $\mu=0, \nu=0$ component of (21), including terms up to mass dimension 6. Tensor symmetry properties of the coefficients in (21) can be used to eliminate some contributions outright (see the Young tableau in table 1 of [45] and the appendix of this paper (59)). For instance, antisymmetry of the indices yields $\hat{s}^{0000}=0=\hat{s}^{000i}$ and $\hat{q}^{000i}=0$. The surviving contributions to the 00 component of (21) are initially collected as

$$\delta M^{00\rho\sigma} h_{\rho\sigma} = -\frac{1}{2} k^{(6)0i0j0k0l} \partial_{ijkl} h_{00} - \left\{ \frac{1}{2} k^{(6)0j0k0lim} \partial_{jklm} + \frac{1}{4} q^{(5)0ij0k0l} \partial_{jkl} \right\} h_{0i}$$

$$- \left\{ \frac{1}{2} \left[s^{(4)0ik0jl} \partial_{kl} + s^{(6)0ik0jlmn} \partial_{klmn} + k^{(6)0k0limjn} \partial_{klmn} \right] \right.$$

$$+ \frac{1}{4} \left[q^{(5)0ik0ljm} + q^{(5)0jk0lim} \right] \partial_{klm} \right\} h_{ij}$$
(22)

where we make use of a short-hand $(\partial_{ijk...} = \partial_i \partial_j \partial_k...)$ for multiple partials. Among the coefficients occurring in (22), those that are isotropic will be invariant under observer rotations SO(3), and thus expressible in terms of rotational scalar contractions, the kronecker delta δ^{ij} and the levi-civita ϵ^{ijk} .

As an example of how to decompose the terms in (22), consider the first term on the first line with the coefficients $k^{(6)0i0j0k0l}$, which has ij and kl index symmetry. This would lead us to the only available scalar contractions being $k^{(6)0i0i0j0j}$ and $k^{(6)0i0j0i0j}$. However, because the underlying tensor satisfies the cyclic identity $k^{(6)\mu\epsilon_1\nu\epsilon_2\rho\epsilon_3\sigma\epsilon_4} + k^{(6)\mu\epsilon_1\nu\epsilon_3\epsilon_2\rho\sigma\epsilon_4} + k^{(6)\mu\epsilon_1\nu\rho\epsilon_2\epsilon_3\sigma\epsilon_4} = 0$, one can show that $k^{(6)0i0j0i0j} = k^{(6)0i0i0j0j}$. Therefore the $k^{(6)0i0j0j0l}$ coefficients, in the isotropic limit, must be proportional to combinations of kronecker deltas $\delta^{ij}\delta^{kl} + \ldots$ and the one scalar $k^{(6)0i0i0j0j}$. Symmetry considerations lead us to

$$k^{(6)0i0j0k0l} = \frac{1}{15} (\delta^{ij} \delta^{kl} + \delta^{ik} \delta^{jl} + \delta^{il} \delta^{jk}) k^{(6)0m0m0n0n},$$
(23)

and thus

$$-\frac{1}{2}k^{(6)0i0j0k0l}\partial_{ijkl}h_{00} = -\frac{1}{10}k^{(6)0m0m0n0n}\nabla^4h_{00}, \tag{24}$$

which simplifies the first term in (22) to the desired form.

For the second line in (22), the coefficients $k^{(6)0j0k0lim}$ and $q^{(5)0ij0k0l}$ do not appear to have any scalar contractions due to the number of indices, or the symmetry properties. Nor can they be written in terms of purely δ_{ij} and ϵ_{ijk} . We conclude their isotropic limit contribution vanishes:

$$-\left\{\frac{1}{2}k^{(6)0j0k0lim}\partial_{jklm} + \frac{1}{4}q^{(5)0ij0k0l}\partial_{jkl}\right\}h_{0i} \stackrel{\text{iso}}{=} 0.$$
 (25)

One proceeds along similar lines for the remaining terms in (22). The details are relegated to the appendix.

The final simplification to the isotropic coefficient case for (22) results in

$$\delta M^{00\rho\sigma} h_{\rho\sigma} = -\frac{1}{10} k^{(6)0m0m0n0n} \nabla^4 h_{00} + \left\{ \frac{1}{12} s^{(4)0kl0kl} + \frac{1}{30} s^{(6)0kl0klmm} \nabla^2 + \frac{1}{30} k^{(6)0k0klmlm} \nabla^2 \right\} \times (\partial_i \partial_j - \delta^{ij} \nabla^2) h_{ij}.$$
(26)

Note the absence of the h_{0i} components in this case. The remaining components of (21) $\mu = 0, \nu = i$ and $\mu = i, \nu = j$ are worked out in the appendix. The equation for h_{0i} decouples from the remaining components of $h_{\mu\nu}$ and we display below the coupled equations for the components h_{00} and h_{jj} . As in the special case of the previous section, the off-diagonal components of h_{ij} can be obtained from a traceless version of appendix (65), of secondary interest in this work.

To obtain the relevant differential equations we make the partial choice of gauge: $\partial_j h_{ij} = \partial_i (h_{jj} - h_{00})/2$. Furthermore, it will be convenient for solving the differential equations to work with the trace-reversed components $\bar{h}_{00} = (1/2)(h_{00} + h_{jj})$ and $\bar{h}_{jj} = (1/2)(3h_{00} - h_{jj})$. Also, since they can be probed with other tests [48], we disregard the mass dimension 4 isotropic coefficients. With these choices and the results of the appendix, the two coupled equations are given by,

$$-\frac{1}{2}\left[\nabla^2 + (k_1 + k_2)\nabla^4\right]\bar{h}_{00} - \frac{1}{2}k_1\nabla^4\bar{h}_{jj} = 8\pi G_N\rho,\tag{27}$$

$$-\frac{1}{2}\left[\nabla^2 + k_2\nabla^4\right]\bar{h}_{ii} - \frac{1}{2}(k_2 + k_3)\nabla^4\bar{h}_{00} = 0, \tag{28}$$

where the k_1 , k_2 , and k_3 are the combinations

$$k_{1} = \frac{1}{10}k^{(6)0i0i0j0j},$$

$$k_{2} = \frac{1}{15}[s^{(6)0kl0klmm} + k^{(6)0k0klmlm}],$$

$$k_{3} = \frac{1}{18}s^{(6)klmklmnn} + \frac{1}{15}k^{(6)klklmnmn}.$$
(29)

These equations are very similar to those in (9), except that now we have three *a priori* independent combinations of coefficients, instead of two. The combinations appearing in (29) overlap with the isotropic coefficient combination appearing in GW tests, which is in appendix (67).

It is important to emphasize that the assumption of isotropy in a special coordinate system is a special case of the general coefficients in the EFT framework. The focus here is on these particular coefficients, effectively setting the others to zero. However, in principle one can use the coordinate covariance of the EFT to transform the coefficients from one frame to another. Isotropic coefficients are rotational scalars. Under SO(3) rotations of the spatial coordinates $(x')^j = R_k^j x^k$ they do not change. Under observer boosts, however, the components would mix with others. Once one introduces a boost velocity β , this is typically of order 10^{-4} , and to be consistent one needs the full post-Newtonian metric with includes the velocity of matter v^j included. We do not consider this here but it has been done elsewhere for coefficients in the gravity sector [35, 47, 88].

3.2.2. Solving the coupled equations. With a similar approach to section 3.1, we seek Green function solutions for a unit point source $4\pi G_N \rho = \delta^{(3)}(\vec{R})$, and choose boundary conditions so that the fields vanish at spatial infinity. Denoting the Green functions for \bar{h}_{00} and \bar{h}_{jj} as G_1 and G_2 , respectively, we obtain the Green function matrix equation,

$$\begin{pmatrix} \nabla^2 + (k_1 + k_2)\nabla^4 & k_1\nabla^4 \\ (k_2 + k_3)\nabla^4 & \nabla^2 + k_2\nabla^4 \end{pmatrix} \begin{pmatrix} G_1 \\ G_2 \end{pmatrix} = \begin{pmatrix} -4\delta^{(3)}(\vec{R}) \\ 0 \end{pmatrix}.$$
(30)

Next we use Fourier transforms of the Green functions via

$$G_n = \frac{1}{(2\pi)^3} \int d^3p e^{i\vec{p}\cdot\vec{R}} \tilde{G}_n, \tag{31}$$

where $n = \{1, 2\}$. With this, the matrix equation becomes algebraic in momentum space as

$$\begin{pmatrix} -1 + (k_1 + k_2)p^2 & k_1p^2 \\ (k_2 + k_3)p^2 & -1 + k_2p^2 \end{pmatrix} \begin{pmatrix} p^2 \tilde{G}_1 \\ p^2 \tilde{G}_2 \end{pmatrix} = \begin{pmatrix} -4 \\ 0 \end{pmatrix}, \tag{32}$$

where $p = |\vec{p}|$ and p^2 is factored from the matrix to make it unitless. Since it is of crucial importance for the pole structure and the solutions, we record here the determinant of the matrix M in (32):

$$\det M = 1 - (k_1 + 2k_2)p^2 + (k_2^2 - k_1k_3)p^4. \tag{33}$$

Inverting the matrix in (32), we obtain the momentum space solutions:

$$\tilde{G}_{1} = \frac{4(1 - k_{2}p^{2})}{p^{2} \det M},
\tilde{G}_{2} = \frac{4(k_{2} + k_{3})}{\det M}.$$
(34)

Inserting the results into (31), and taking advantage of the spherically symmetric nature of the solutions in (34), we can directly integrate the angular part via $d^3p = p^2dpd\Omega_p$, What remains is a one-dimensional Fourier transform integral over the magnitude of the momentum p. For instance, for G_1 we obtain

$$G_1 = -\frac{i}{\pi^2 R} \int_{-\infty}^{\infty} e^{ipR} \frac{1 - p^2 k_2}{p[1 - (k_1 + 2k_2)p^2 + (k_2^2 - k_1 k_3)p^4]} dp, \tag{35}$$

with a similar integral for G_2 . This integral may be evaluated using contour integration in complex p space. Clearly the poles of (33) play a strong role.

The result of the complex integration calculation gives the Green functions G_1 and G_2 in position space. We find,

$$G_{1} = \frac{1}{\pi R} \left[1 + \frac{1}{2} \left(\frac{\zeta_{1} \zeta_{\alpha}}{\sqrt{1 + 4\chi}} - 1 \right) e^{\pm iw_{1}R} - \frac{1}{2} \left(\frac{\zeta_{1} \zeta_{\alpha}}{\sqrt{1 + 4\chi}} + 1 \right) e^{\pm iw_{2}R} \right],$$

$$G_{2} = \frac{\chi \zeta_{1} \zeta_{\alpha}}{\sqrt{1 + 4\chi} \pi R} (e^{\pm iw_{1}R} - e^{\pm iw_{2}R}),$$
(36)

where we define χ , the poles w_1 and w_2 , and the 'zetas' as

$$\chi = \frac{k_2 + k_3}{k_1},\tag{37}$$

$$w_{1} = \frac{1}{\sqrt{2|k_{2}^{2} - k_{1}k_{3}|}} \left(\zeta_{\alpha}(k_{1} + 2k_{2}) + |k_{1}|\sqrt{1 + 4\chi} \right)^{1/2},$$

$$w_{2} = \frac{1}{\sqrt{2|k_{2}^{2} - k_{1}k_{3}|}} \left(\zeta_{\alpha}(k_{1} + 2k_{2}) - |k_{1}|\sqrt{1 + 4\chi} \right)^{1/2},$$
(38)

$$w_2 = \frac{1}{\sqrt{2|k_2^2 - k_1 k_3|}} \left(\zeta_\alpha(k_1 + 2k_2) - |k_1| \sqrt{1 + 4\chi} \right)^{1/2},\tag{39}$$

$$\zeta_1 = \operatorname{sign}(k_1), \tag{40}$$

$$\zeta_{\alpha} = \operatorname{sign}(k_2^2 - k_1 k_3). \tag{41}$$

The \pm signs in the exponential functions are to be chosen to ensure an exponential decay rather than growth, and the choice depends on the sign of the complex part of w_1 and w_2 .

Examination of the solutions (36) reveals that the amplitudes of the exponential terms appear to become arbitrarily large as $\chi \to -1/4$ from above or below. However, in the same limit we have w_1 appearing to coincide with w_2 , and so the two terms in (36) appear as though they might cancel. So it is not immediately clear the behavior of the solution in this limit. To understand the general solution better, we explore some limiting cases.

3.2.3. Exploration of solutions. First, we will focus the attention on the combination of the Green functions related to the Newtonian potential, $\mathcal{G}_1 = (1/2)(G_1 + G_2)$. This simplifies to

$$G_{1} = \frac{1}{2\pi R} \left[1 + \frac{1}{2} \left(\frac{\zeta_{1}\zeta_{\alpha}(1+2\chi)}{\sqrt{1+4\chi}} - 1 \right) e^{\pm iw_{1}R} - \frac{1}{2} \left(\frac{\zeta_{1}\zeta_{\alpha}(1+2\chi)}{\sqrt{1+4\chi}} + 1 \right) e^{\pm iw_{2}R} \right]. \quad (42)$$

Note that this solution reduces to the one appearing in the prior section 3.1 with the substitutions $k_1 = k_{ll}/3 - k_{00}$, $k_2 = k_{00} - k_{ll}$, and $k_3 = 8k_{ll}/3$. The Newtonian potential for a realistic source is obtained from the matter distribution integral (19).

Consider a sample case of the k_1 , k_2 , and k_3 parameter space. Let $\chi = -6/25$ so that $\sqrt{1+4\chi} = 1/5$. Then we further specialize to the case $k_3 = 0$. Inserting these assumptions into (42) leaves a solution valid for a one parameter subset (chosen as k_2). Specifically we find

$$\mathcal{G}_{1} = \begin{cases} \frac{1}{2\pi R} \left(1 - \frac{9}{5} e^{-R/\lambda_{1}} + \frac{4}{5} e^{-R/\lambda_{2}} \right), & k_{2} > 0 \\ \frac{1}{2\pi R} \left(1 - \frac{9}{5} e^{\mp iR/\lambda_{1}} + \frac{4}{5} e^{\mp iR/\lambda_{2}} \right), & k_{2} < 0 \end{cases}$$

$$(43)$$

where the length scales are $\lambda_1 = \sqrt{3|k_2|/2}$ and $\lambda_2 = \sqrt{2|k_2|/3}$. Note that in this case, with a negative sign for k_2 , one obtains purely oscillatory corrections with no exponential damping. For this latter case, if desired one can obtain a real solution by superposition of the two signs.

If the length scale of the coefficients, $\lambda \sim \sqrt{|k_2|}$, are expected to be small compared to accessible laboratory length scales than the solution for $k_2 > 0$ is consistent with a new force that arises only on short scales. This situation is consistent with the spacetime symmetry breaking being small, and the terms added to the action being small corrections to known physics. On the other hand, if $k_2 < 0$, with small length scales λ , one finds a rapidly spatially varying Newtonian potential with a substantial (of order unity or higher) amplitude. The lack of such observed long range forces could be used to theoretically reject this region of the coefficient space of solutions as unphysical. Note that this latter case bears similarity to considerations of higher derivative models where, in some cases, one does not find a smooth limit to a perturbative approach [89, 90]. Similarly here, trying extrapolate $k_2 \to 0$ when $k_2 < 0$ simply results in rapidly varying (unobserved) forces. In contrast, again, the former solution $k_2 > 0$ with the decaying exponential reduces to a delta function at the origin when $k_2 \to 0$, like the contact term found by a perturbative approach in [16]. Such terms also arise in other models [91].

Next we look at what happens when we approach $\chi = -1/4$ from 'below'. Consider $\chi = -13/50$ so that $\sqrt{1+4\chi} = i/5$. Again we assume $k_3 = 0$ and we obtain in this case,

$$\mathcal{G}_{1} = \begin{cases} \frac{1}{2\pi R} \left(1 - e^{-R/\lambda_{1}} \left[\cos(R/\lambda_{2}) + \frac{12}{5} \sin(R/\lambda_{2}) \right] \right), & k_{2} > 0 \\ \frac{1}{2\pi R} \left(1 - e^{-R/\lambda_{2}} \left[\cos(R/\lambda_{1}) - \frac{12}{5} \sin(R/\lambda_{1}) \right] \right), & k_{2} < 0 \end{cases}$$
(44)

where now $\lambda_1 = \sqrt{26|k_2|/25}$ and $\lambda_2 = \sqrt{26|k_2|}$. We now have a damped exponential behavior accompanied with oscillatory behavior in R. Changing the sign of k_2 merely swaps the length scales involved in damping versus oscillations. We plot the cases described above in (43) and (44) in figure 2. All of the examples exhibit behavior strikingly different from the Newtonian case. Note in particular, a resemblance of the modified Newtonian potential solutions in (44) to a Dilaton-gravity coupling proposed long ago [2].

Returning to the general case of (42), we enumerate the different functional forms of the solution for different regions of the space spanned by the coefficients k_1 , k_2 , k_3 in table 1. We assume that we do not make contact with the singular point in w (41), $k_2^2 = k_1 k_3$, as this point would correspond to the disappearance of the p^4 term in (33), and would impose a condition on the *a priori* independent coefficients. Nonetheless we include this case in the appendix 'Special

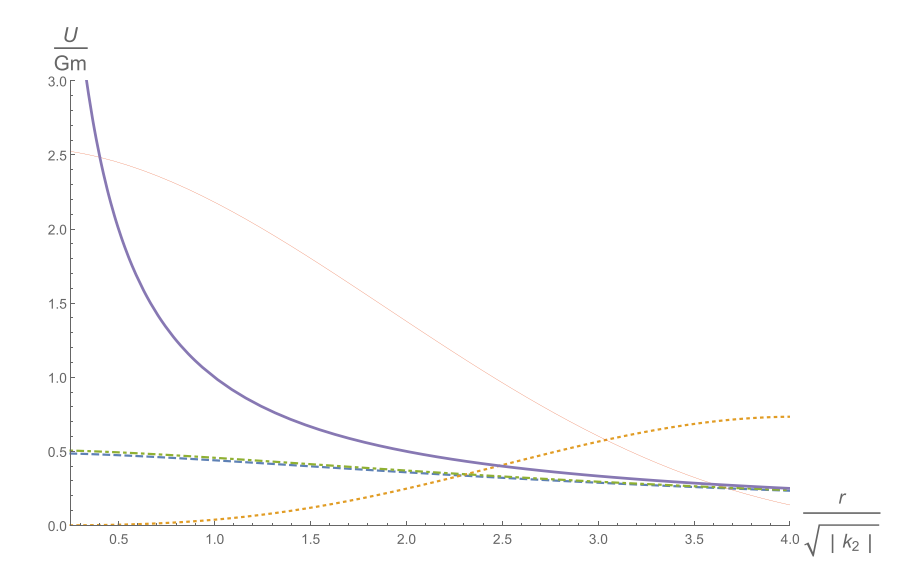


Figure 2. A plot of the modified potential of equations (43) and (44) for a unit mass at the origin (r=0). The vertical axis is the scaled potential and the horizontal axis is the distance from the source in terms of the length unit $\sqrt{|k_2|}$. The solid curve is the Newtonian potential 1/r falloff. The dashed and dotted curves are the solutions in equation (43), with $\chi = -6/25$ and $k_2 > 0$ and $k_2 < 0$, respectively. The dot-dashed and thin curves are the solutions from equation (44) for $\chi = -13/50$, again with $k_2 > 0$ and $k_2 < 0$, respectively.

Table 1. Four cases of the general solution (42) for the Newtonian potential Green function \mathcal{G}_1 , categorized by conditions on the coefficient combinations k_1, k_2 , and k_3 . Here $a=\zeta_\alpha(k_1+2k_2)$ and $b=|k_1|\sqrt{1+4\chi}$. The length scales are $\lambda_\pm=\sqrt{\frac{2|k_2^2-k_1k_3|}{|a\pm b|}}$ and $\lambda_{1,2}=2\sqrt{\frac{(k_2^2-k_1k_3)}{(2\sqrt{(k_2^2-k_1k_3)}-k_1-2k_2)}}$. For the last row, the case of $\chi+\frac{1}{4}<0$ implies $k_2^2-k_1k_3>0$.

$\overline{\mathcal{G}_1}$	$\mathrm{sign}(\chi+\tfrac{1}{4})$	a, b cond.
$rac{1}{2\pi R}\left[1+rac{1}{2}\left(rac{\zeta_1\zeta_lpha(1+2\chi)}{\sqrt{1+4\chi}}-1 ight)e^{\pm iR/\lambda}+ ight.$	+	$\left \frac{a}{b}\right < 1$
$-\frac{1}{2}\left(\frac{\zeta_1\zeta_\alpha(1+2\chi)}{\sqrt{1+4\chi}}+1\right)e^{-R/\lambda}\right]$		
$\frac{1}{2\pi R}\left[1+\frac{1}{2}\left(rac{\zeta_1\zeta_lpha(1+2\chi)}{\sqrt{1+4\chi}}-1 ight)e^{\pm iR/\lambda}+ ight.$	+	$\frac{a}{b} > 1$
$-\frac{1}{2}\left(\frac{\zeta_1\zeta_\alpha(1+2\chi)}{\sqrt{1+4\chi}}+1\right)e^{\pm iR/\lambda}$		
$\frac{1}{2\pi R} \left[1 + \frac{1}{2} \left(\frac{\zeta_1 \zeta_\alpha (1 + 2\chi)}{\sqrt{1 + 4\chi}} - 1 \right) e^{-R/\lambda} + \right]$	+	$\frac{a}{b} < -1$
$-\frac{1}{2}\left(\frac{\zeta_1\zeta_{lpha}(1+2\chi)}{\sqrt{1+4\chi}}+1 ight)e^{-R/\lambda}$		
$\frac{1}{2\pi R} - \frac{1}{2\pi R} \exp\left(-\frac{R}{\lambda_1}\right) \left[\cos\left(\frac{R}{\lambda_2}\right) - \frac{\zeta_1(1+2\chi)}{\sqrt{ 1+4\chi }} \sin\left(\frac{R}{\lambda_2}\right)\right]$	_	N/A

cases: $k_2^2 - k_1 k_3 = 0 \lor k_1 + 2k_2 = 0$ ' since it may be of interest. Also, as in section 3.1, we can explore what happens near the apparent singularity in the solution (42), and this is discussed in appendix 'Large amplitude limit of the solution'.

To end this subsection, we revisit the equation (28) using a perturbative method adopted in past works. This method amounts to assuming the metric components can be obtained from a series $h_{\mu\nu} = h_{\mu\nu}^{(0)} + h_{\mu\nu}^{(1)} + \dots$ We assume that the 0th order, GR solution, satisfies equations (28) for the case of vanishing k_1 , k_2 , and k_3 . Next we solve for the first correction to this solution $h_{\mu\nu}^{(1)}$. Using this method, we find the zeroth and first correction for h_{00} to be given by

$$h_{00} = 2U_0 + \kappa (k_1 + 2k_2 + k_3)\rho, \tag{45}$$

where U_0 is the usual Newtonian potential from a mass density ρ and the first order correction is a contact term that is nonvanishing only within the mass distribution [16, 91]. The first order solution (45) can be contrasted with the results of table 1. Clearly the solutions in table 1 represent a more detailed, careful look at the effects of the isotropic coefficients in (29).

4. Anisotropic exact solutions

While not the main focus of the paper, we discuss features of exact solutions when the coefficients are anisotropic. In the special limit that the only nonzero coefficients in (21) are $k^{(6)0i0j0k0l}$, and still assuming the static matter situation, the equations for h_{jj} and h_{00} can be decoupled. In this case the equation satisfied by h_{00} is given by

$$-\nabla^2 h_{00} - \frac{1}{2} k^{(6)0i0j0k0l} \partial_{ijkl} h_{00} = 8\pi G_N \rho. \tag{46}$$

An equation of this form was the subject of [16, 17], where a perturbative approach to the solution was taken (with the result contained in (6)). In the perturbative approach, the second term in (46) is treated as much less than the first term, and a zeroth order solution is inserted in for h_{00} in that term. As one of the goals in this paper is to examine the exact, nonperturbative solutions, we attempt here to look at anisotropic cases.

It turns out, exact analytic solutions for (46) for the 15 independent components of an arbitrary $k^{(6)0i0j0k0l}$ are quite challenging. Instead we examine a special case to show the features of such solutions. We adopt a case where $k^{(6)0i0j0k0l}$ can be written in terms of a contraction $K^{ij} = k^{(6)0i0j0k0k}$ and its trace K^{jj} . This reduces (46) to the form,

$$-\nabla^2 (1 + \frac{3}{7} K^{ij} \partial_{ij} - \frac{3}{70} K^{jj} \nabla^4) h_{00} = 8\pi G_N \rho. \tag{47}$$

Next we assume only diagonal elements K^{xx} , K^{yy} , and K^{zz} , such that $K^{xx} = K^{yy} = K^{zz}/18$, then the equation can be written in the simpler form,

$$\nabla^2 (1 - \lambda^2 \partial_z^2) h_{00} = -8\pi G_N \rho, \tag{48}$$

where $\lambda = \sqrt{8|K_{zz}|/21}$ and $K_{zz} < 0$, so one independent coefficient is left. As before, we construct the Green function solution for a point source. By writing the Green function version of equation (48) as two equations $(1 - \lambda^2 \partial_z^2)\Phi = -\delta^{(3)}(\vec{r})$ and $\nabla^2 \mathcal{G} = \Phi$, which can be solved separately [92, 93], and then combining the results, we reduce the answer to an integral over one variable:

$$\mathcal{G}(\rho, z) = \frac{1}{8\pi\lambda} \int_{-\infty}^{\infty} dz' \frac{e^{-|z'|/\lambda}}{\sqrt{\rho^2 + (z - z')^2}},\tag{49}$$

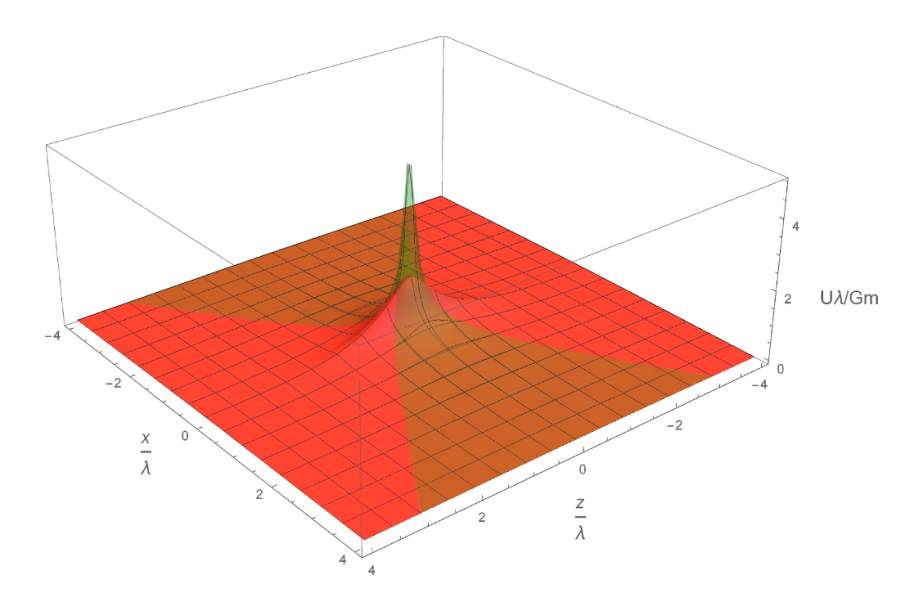


Figure 3. Plot of the scaled anisotropic potential of (49) (damped case), shown in light red versus the Newtonian potential, in transparent green. The source is a point mass at the origin. The behavior is the same in the y direction by the azimuthal symmetry of (49).

where we adopt cylindrical coordinates ρ , ϕ , z and $K_{zz} < 0$. If instead we consider the case of $K_{zz} > 0$, there is a sign change in (49) and the integral changes to

$$\mathcal{G}(\rho, z) = \frac{-i}{8\pi\lambda} \int_{-\infty}^{\infty} dz' \frac{e^{i|z'|/\lambda}}{\sqrt{\rho^2 + (z - z')^2}}.$$
 (50)

We have been unable to evaluate these integrals analytically, so we take a numerical approach. In the figures 3 and 4, we plot the results from (49) and (50). The standard Newtonian result 1/r is plotted along with a numerical evaluation of (49) and (50). In the case of the damped-type solution in (49), we see a narrowed or cuspy behavior of the potential along the x or y direction, and the amplitude is reduced. In the other case of the oscillating-type solution in (50), we see large oscillations along the z direction that do not fall off rapidly.

To contrast with the numerically generated (49) and (50), we outline some features of the perturbative approach. The idea is to solve for the Green function iteratively $\mathcal{G} = \mathcal{G}_{(0)} + \mathcal{G}_{(1)} + \mathcal{G}_{(2)} + \ldots$, where the subscript indicates powers of λ^2 . The equations for the 0 th and subsequent orders are given by

$$\nabla^{2}\mathcal{G}_{(0)} = -\delta^{(3)}(\vec{r}),$$

$$\nabla^{2}\mathcal{G}_{(1)} = \lambda^{2}\partial_{z}^{2}\nabla^{2}\mathcal{G}_{(0)},$$
...
$$\nabla^{2}\mathcal{G}_{(n)} = \lambda^{2n}\partial_{z}^{2n}\nabla^{2}\mathcal{G}_{(n-1)}.$$
(51)

This type of approach is what led to the results in equation (6), where only the first order term is used but arbitrary coefficients assumed.

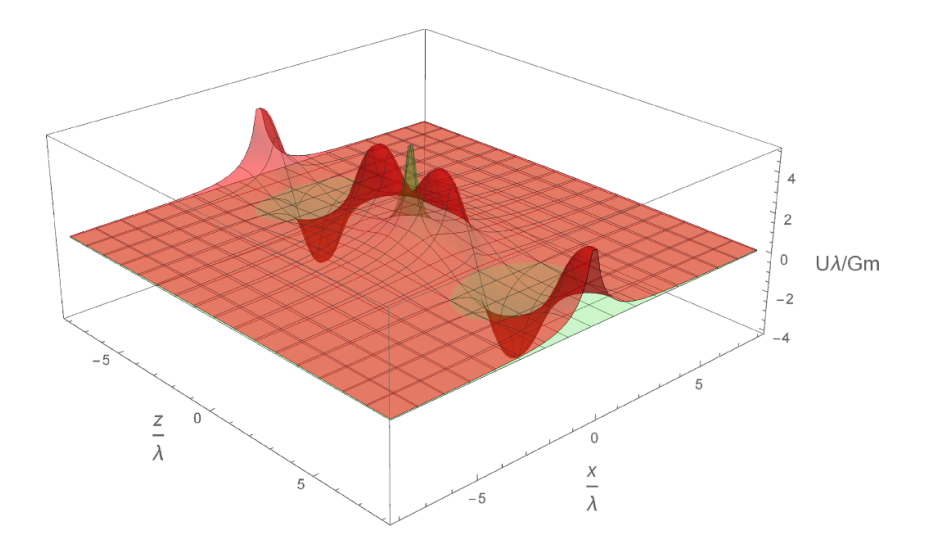


Figure 4. Plot of the scaled anisotropic potential of (50) (oscillating case), shown in light red versus the Newtonian potential, in transparent green. The source is a point mass at the origin. The behavior is the same in the y direction by the aximuthal symmetry of (50).

The *n*th term in the series (51) can be solved by using standard results for the derivatives of 1/r [94]. For $\mathcal{G}_{(n)}$ we find

$$G_{(n)} = \frac{\lambda^{2n}}{4\pi} \frac{(4n-1)!!}{r^{2n+1}} n^{\langle zzz...\rangle},$$
(52)

where $n^j = r^j/r$ is a unit vector and $n^{< jkl ...>}$ is a symmetric trace free (STF) tensor formed from unit vectors and δ^{ij} (for example, $n^{< jk>} = n^j n^k - (1/3)\delta^{ij}$). The STF tensor in (52) is to be evaluated along the z direction. Note that the convergence of such a series is not clear, since, for example, the size of successive terms grow with n.

To illustrate this, we plot the exact numerical evaluation of (49) with the successive approximations (51). Figure 5 shows the approximations up to the third term in the series. While the approximations approach the exact answer as x/λ decreases, they vary considerably at scales of order $x \sim \lambda$. In fact, it appears successive terms added to the first $G_{(1)}$ are worse than the just the first approximation alone!

From this brief study we can draw several conclusions and open an area for future work. We find that in the case of the damped exponential, where the equation to solve is $(1-\lambda^2\partial_z^2)\nabla^2\mathcal{G}_1=-\delta^{(3)}(\vec{r})$, the first order approximation follows the exact solution until the ρ and z reach the scale of λ . This behavior is expected and justifies the use of the perturbative method generally. On the other hand we see from figure 5, successive terms in a series (51) appear to fail to converge to the exact result. It would be of interest to study in detail how well these approximations could follow an exact solution in general.

Of course, without knowing the true nature of the Newtonian level potential at short ranges from an unknown fundamental theory, we can only speculate. Suppose, hypothetically, that the potential in equations (49) or (50) was indeed the potential coming from an underlying theory of physics. The question then is how well a perturbative approach could match this in the appropriate range. We see above that for some choices of constants, the perturbative approach does not capture the behavior correctly. However, there is an important caveat to include. We truncated the expansion in (3.2) to mass dimension 6. In the perturbative approach, beyond a

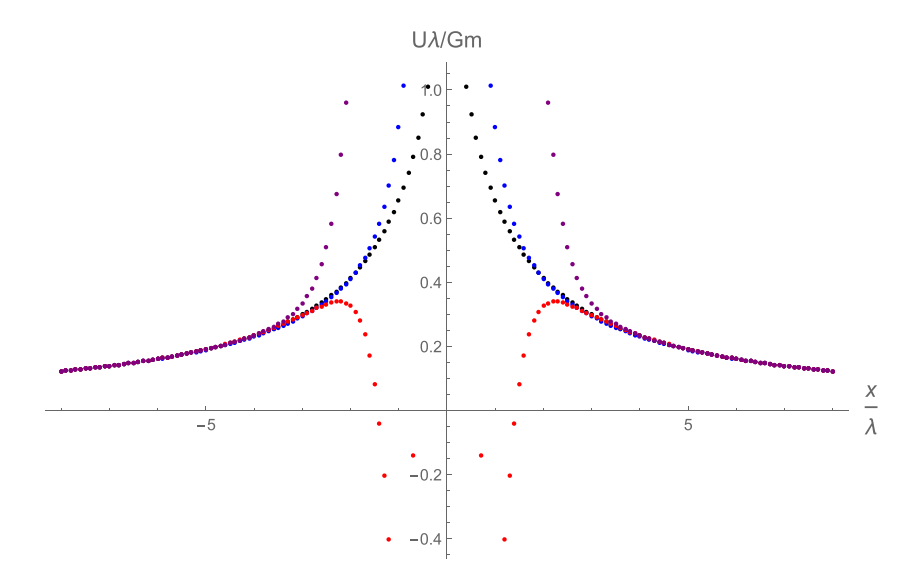


Figure 5. Plot of the potential of (49) along with successive approximations in a perturbative scheme from (51). In black is the exact solution, blue is the first approximation $\mathcal{G}_0 + \mathcal{G}_1$, red is the second approximation $\mathcal{G}_{(0)} + \mathcal{G}_{(1)} + \mathcal{G}_{(2)}$, and purple is $\mathcal{G}_{(0)} + \mathcal{G}_{(1)} + \mathcal{G}_{(2)} + \mathcal{G}_{(3)}$.

first order approximation to the equation $(1 + \lambda^2 \partial_z^2) \nabla^2 \mathcal{G}_1 = -\delta^{(3)}(\vec{r})$, would necessitate the inclusion of mass dimension 8 terms in the action, for consistency. Indeed, it could be that higher order terms in the action could contribute to an approximation scheme, and provide 'counterterms' that result in smooth connection to the underlying potential [95]. For example, imposing requirements term by term in a series expansion, could place theoretical constraints on the coefficients themselves. It would be of interest to attempt a general study of this in gravity or other sectors like the photon sector. Furthermore, this paper studies only the static limit, so it is of interest to study these issues in the time-dependent limit.

Currently, experimental constraints on many of the anisotropic coefficients already exist using experiments that satisfy the experimental constraint of being sensitive enough to measure the Newtonian forces between test masses [96]. Thus if we assume that the perturbative approach is valid, then the coefficient space for anisotropic coefficients is well covered in SR gravity tests [81, 82, 84, 97].

5. Experimental implications

Typical short range gravity tests are designed to measure the attraction between two masses, for instance two flat plates [96, 98]. To see what implications the results of section 3 have on experimental signatures, we plot the gravitational field above a circular disk of mass (figure 6). We include the cases of the Newtonian gravity, the Yukawa potential term (18), and the four sample cases of spacetime-symmetry breaking of equations (43) and (44) and display the vertical component in figure 7.

It is clear that the cases studied here exhibit behavior quite different from the Yukawa parametrization. The Yukawa parametrization shows a deviation from the Newtonian case with the force becoming stronger on shorter scales, as expected. The different Lorentz violation cases

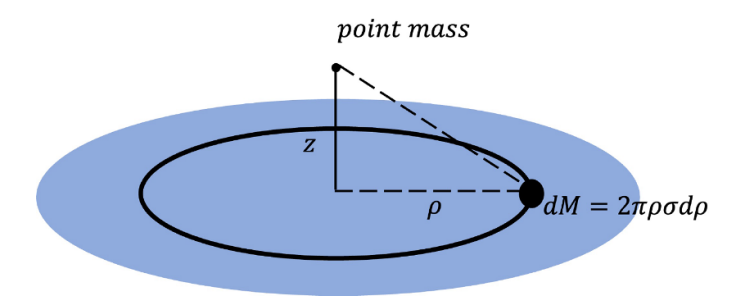


Figure 6. A point mass lies above a thin disk of mass. The gravitational field $\vec{g} = \vec{\nabla} U$ is integrated over this distribution.

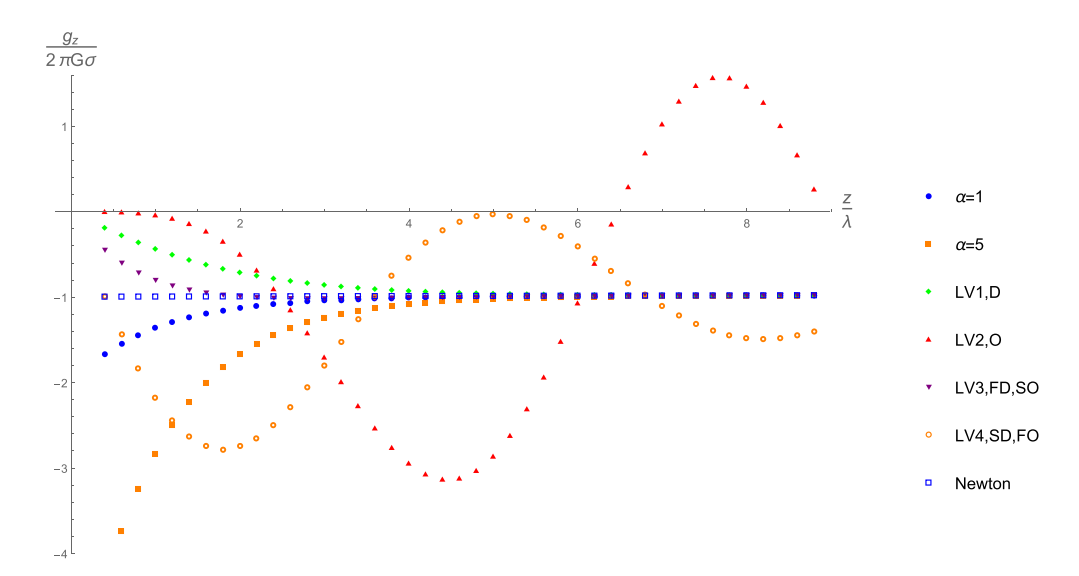


Figure 7. A plot of the gravitational field $g_z = \partial U/\partial z$ at a point above the center of a large flat disk of mass. We include two samples of the Yukawa force with $\alpha=1,5$ and the four types of solutions in equations (43) and (44). The vertical axis is the scaled gravitational field and the horizontal axis is the height above the disk z in units relative to the length scale λ . We set the scale of Lorentz violation to be $\sqrt{|k_2|} = \lambda$. The four cases of Lorentz violation show damping only (D), oscillation only (O), and fast damping (FD) with slow oscillation (SO) and finally slow damping (SD) with fast oscillation (FO).

have oscillatory behavior with and without damping. To get an idea how analysis might proceed, we produce the same plot with one of the four cases, the damped and oscillating solution, but with varying values of $|k_2|$, in plot 8. As $|k_2|$ becomes smaller, the effects deviating from the Newton case narrow to a region at smaller and smaller length scales. This shows that some of the solutions have the feature that $|k_2|$ could be constrained to be below a certain length scale. For example, we can make a crude estimate from figures 7 and 8: if the Yukawa-type force has been constrained to a region of standard $\alpha - \lambda$ space where $\alpha \sim 1$ and $\lambda \sim 200~\mu\text{m}$, like the experiment in [1], than roughly $\sqrt{k_2} < 200~\mu\text{m}$, if one used the specific case of (43).

However, what we plot here in figure 8 is only a one coefficient special case, in the full model one could use each of the cases in table 1 to fit data and rule out a region of $k_1 - k_2 - k_3$ space, similar to the way exclusion regions are mapped out in $\alpha - \lambda$ plots in the experimental

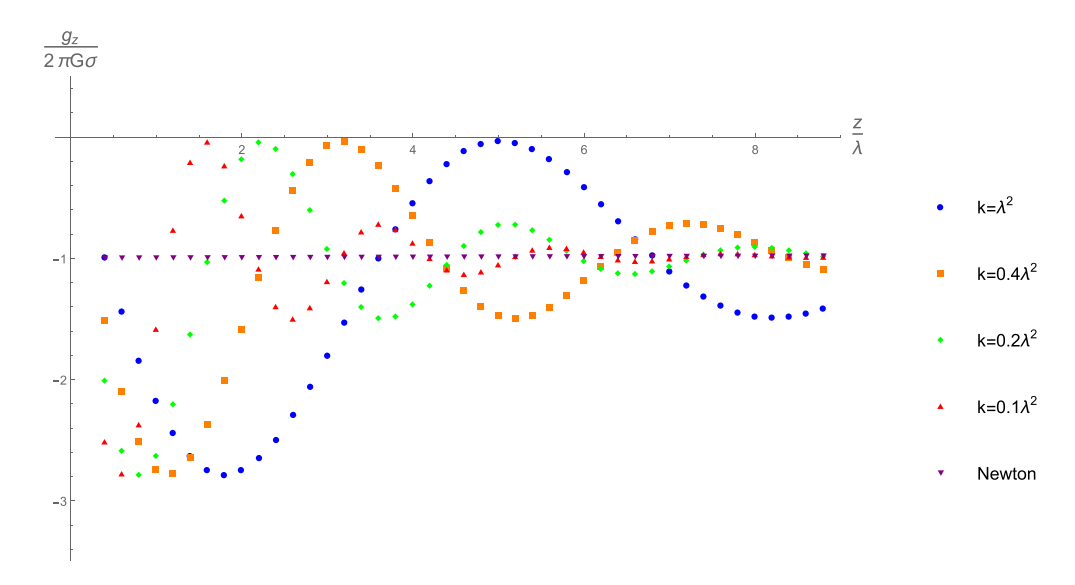


Figure 8. A plot of the gravitational field $g_z = \partial U/\partial z$ at a point near a large flat plate of mass. In this plot we let k_2 vary and show the effect on the damped and oscillating solution from equation (44).

literature. In general, the region of $k_1 - k_2 - k_3$ affects the amplitude of the exponential and oscillatory terms and the length scales involved, as can be seen from table 1.

6. Summary and outlook

In this paper, we studied SR gravity signals for Lorentz violation that go beyond the leading order approximation, by taking a non-perturbative approach. The focus was on isotropic coefficients, since they are generally harder to measure in experiments and observations. The main results are the coupled field equations for the metric components h_{00} and h_{jj} in the static limit, equations (28), and the general solution for the Green function \mathcal{G}_1 for $h_{00} = 2U$, organized into four cases in table 1.

These solutions go beyond the standard Yukawa parametrization (18) and could be studied in SR gravity tests of all kinds. Particularly, it may be of interest for SR tests that probe large non-Newtonian forces. One option for data analysis is to restrict attention to the solutions in the last two rows in table 1, which do not exhibit undamped oscillations. One could then attempt to use experimental data to measure the coefficient combinations k_1 , k_2 , and k_3 (equation (29)) contained in these expressions. Analysis could also proceed with a simpler two coefficient special case model in section 3.1, or, in the case of tests sensitive to very large non-Newtonian forces, one could use the large amplitude, $\chi = -1/4 + \epsilon$ limit, outlined in the appendix and table 4.

The isotropic mass dimension 6 coefficients that can be probed using the solutions in this work, in equation (29), appear to be distinct combinations from the combination appearing in GW propagation tests [99], as shown in (67). This demonstrates the usefulness of additional SR gravity test analysis outlined in this work, providing an independent probe of isotropic coefficients from GW tests.

In this work, we also collect some useful pedagogical results with explicit examples of the construction of isotropic coefficients from Young tableau, as discussed in appendix 'Isotropic limit of coefficients'. In section 4 we discussed exact solutions in the case of anisotropic coefficients, and compared the results to perturbative methods used so far. It would be of interest to compute integrals like (49) and (50) analytically, if possible. In addition, a study of the convergence of the series (51) and related topics like adding time dependence would be of interest. Considerations of this paper could be applied to the photon sector [77, 100], where, analogous to gravity, new types of massive photon-like signals may be revealed.

Data availability statement

No new data were created or analysed in this study.

Acknowledgment

The authors acknowledge support from the National Science Foundation under Grants 1806871 and 2207734. We thank Embry-Riddle Aeronautical University's Undergraduate Research Institute for support of Jennifer L James and Janessa R Slone. Valuable comments on the manuscript have been provided by Brett Altschul, V Alan Kostelecký, and Rui Xu.

Appendix

Special case model

We record the exact field equations for the action in (7), $\mathcal{L} = \frac{1}{2\kappa} \sqrt{-g} \left(R + k_{\alpha\beta} R^{\alpha\beta} R \right)$. Upon variation with respect to the full metric $g_{\mu\nu}$ we obtain:

$$G^{\mu\nu} = \frac{1}{2} g^{\mu\nu} k_{\alpha\beta} R^{\alpha\beta} R - k_{\alpha}^{\mu} R^{\nu\alpha} R - k_{\alpha}^{\nu} R^{\mu\alpha} R - k_{\alpha\beta} R^{\alpha\beta} R^{\mu\nu}$$

$$- \frac{1}{2} g^{\mu\nu} \nabla^{\alpha} \nabla^{\beta} (k_{\alpha\beta} R) - g^{\mu\nu} \nabla^{2} (k_{\alpha\beta} R^{\alpha\beta}) + \frac{1}{2} \nabla_{\alpha} \nabla^{\mu} (k^{\nu\alpha} R)$$

$$+ \frac{1}{2} \nabla_{\alpha} \nabla^{\nu} (k^{\mu\alpha} R) + \nabla^{\mu} \nabla^{\nu} (k_{\alpha\beta} R^{\alpha\beta}) - \frac{1}{2} \nabla^{\alpha} \nabla_{\alpha} (k^{\mu\nu} R).$$

$$(53)$$

Here we treat $k_{\alpha\beta}$ as a fixed background set of coefficients and do not consider field equations obtained with the variation $\delta k_{\alpha\beta}$, but this could be generalized.

Differential equation results

Here we record some basic results that we use in constructing the general solutions for the PDE's in the paper. Boundary conditions are assumed where the fields vanish at spatial infinity. First we note the Helmholtz equation for a field ψ

$$(\nabla^2 + \omega^2)\psi = -\delta^{(3)}(\vec{R}). \tag{54}$$

This is solved with the following Green function (e.g. see [92])

$$\psi = \frac{e^{\pm i\omega R}}{4\pi R}.\tag{55}$$

Note that if ω is a general complex number, $\omega = a + ib$ then one obtains

$$\psi = \frac{e^{\pm iaR}}{4\pi R}e^{\mp bR},\tag{56}$$

which shows that oscillation and damping or growth can occur. When a = 0 and $\mp b < 0$, then the solution to the Proca or modified Helmholtz equation is recovered.

We also record here the less common nonlocal equation considered long ago in generalized electrodynamics [37, 38],

$$(\nabla^2 - \lambda^2 \nabla^4) \psi = -\delta^{(3)}(\vec{R}). \tag{57}$$

For this equation, the Green function is (e.g. see [93]),

$$\psi = \frac{1}{4\pi R} - \frac{e^{-R/\lambda}}{4\pi R}.\tag{58}$$

Here again, λ could be complex, yielding oscillatory behavior.

Isotropic limit of coefficients

We record here the portion of the field equations in the static limit involving the $\delta M^{\mu\nu\rho\sigma}h_{\rho\sigma}$ (definition in equation (21)). It is useful in what follows to enumerate the specific tensor symmetries of the coefficients involved (5). For convenience, we display here the young tableau [45] for the coefficients with spacetime indices:

$$s^{(4)\mu\rho\epsilon\nu\sigma\zeta} \Leftrightarrow \overbrace{\epsilon}^{\mu} \zeta,$$

$$q^{(5)\mu\nu\kappa\alpha\beta\gamma\delta} \Leftrightarrow \overbrace{\kappa}^{\kappa},$$

$$q^{(5)\mu\nu\kappa\alpha\beta\gamma\delta} \Leftrightarrow \overbrace{\kappa}^{\kappa},$$

$$s^{(6)\mu\rho\epsilon\nu\sigma\zeta\alpha\beta} \Leftrightarrow \overbrace{\epsilon}^{\kappa} \zeta,$$

$$k^{(6)\mu\epsilon\nu\zeta\rho\alpha\sigma\beta} \Leftrightarrow \overbrace{\epsilon}^{\kappa} \zeta \alpha \beta.$$

$$(59)$$

Later below, we break down these coefficients into spatial subsets. Young tableau and the process of breaking down tableau into representations of subgroups is described elsewhere [101, 102].

For the space and time components $\delta M^{00\rho\sigma}h_{\rho\sigma}$, $\delta M^{0i\rho\sigma}h_{\rho\sigma}$, and $\delta M^{ij\rho\sigma}h_{\rho\sigma}$, we obtain

$$\delta M^{00\rho\sigma} h_{\rho\sigma} = -\frac{1}{2} k^{(6)0i0j0k0l} \partial_{ijkl} h_{00} - \left\{ \frac{1}{2} k^{(6)0j0k0lim} \partial_{jklm} + \frac{1}{4} q^{(5)0ij0k0l} \partial_{jkl} \right\} h_{0i} - \left\{ \frac{1}{2} \left[s^{(4)0ik0jl} \partial_{kl} + s^{(6)0ik0jlmn} \partial_{klmn} + k^{(6)0k0limjn} \partial_{klmn} \right] + \frac{1}{4} [q^{(5)0ik0ljm} + q^{(5)0jk0lim}] \partial_{klm} \right\} h_{ij},$$
 (60)

$$\begin{split} \delta M^{0i\rho\sigma}h_{\rho\sigma} &= -\{\frac{1}{2}k^{(6)0kil0m0n}\partial_{klmn} - \frac{1}{4}q^{(5)0ik0l0m}\partial_{klmn}\}h_{00} \\ &+ \{\frac{1}{4}[s^{(4)0ik0jl}\partial_{kl} + s^{(6)0ik0jlmn}\partial_{klmn}] - \frac{1}{2}k^{(6)0kilomjn}\partial_{klmn} \\ &- \frac{1}{8}[-q^{(5)0ik0ljm} + q^{(5)0jk0lim} + q^{(5)ijk0l0m}]\partial_{klm}\}h_{0j} \\ &- \{\frac{1}{2}[s^{(4)0jlikm}\partial_{lm} + s^{(6)0jlikmnp}\partial_{lmnp}] + \frac{1}{2}k^{(6)0limjnkp}\partial_{lmnp} \\ &+ \frac{1}{4}[q^{(5)0jlimkn} + q^{(5)ijl0mkn}]\partial_{lmn}\}h_{jk}, \end{split} \tag{61}$$

$$\delta M^{ij\rho\sigma}h_{\rho\sigma} &= -\{\frac{1}{2}[s^{(4)0ik0jl}\partial_{kl} + s^{(6)0ik0jlmn}\partial_{klmn}] + \frac{1}{2}k^{(6)ikjl0m0n}\partial_{klmn} \\ &+ \frac{1}{4}[q^{(5)0ik0ljm} + q^{(5)0jk0lim}]\partial_{klm}\}h_{00} - \{\frac{1}{4}[s^{(4)i0ljkm}\partial_{lm} \\ &+ s^{(6)i0ljkmnp}\partial_{lmnp}] + \frac{1}{4}[i \rightleftharpoons j] + \frac{1}{2}k^{(6)0lkminjp}\partial_{lmnp} \\ &+ \frac{1}{8}[q^{(5)i0ljmkn} + q^{(5)j0limkn} + q^{(5)ikljm0n} + q^{(5)jklim0n}]\partial_{lmn}\}h_{0k} \\ &- \{\frac{1}{2}[s^{(4)ikmjln}\partial_{mn} + s^{(6)ikmjlnpq}\partial_{mnpq}] + \frac{1}{2}k^{(6)imjnkplq}\partial_{mnpq} \\ &+ \frac{1}{4}[q^{(5)ikmjnlp} + q^{(5)jkminlp}]\partial_{mnp}\}h_{kl}, \end{aligned} \tag{62}$$

where we have already used the tensor symmetry properties of the coefficients in (5). To simplify the terms occurring in (62), we assume only isotropic coefficients and express each set of coefficients occurring in (62) in terms of its scalar contractions. To elucidate the process, the results for each of the coefficients are recorded in tables 2 and 3 below. Note that isotropic limits of the coefficients are of interest independently of the present paper. This is due to the challenges of their measurement with the same precision as anisotropic coefficients [103].

The results from the tables 2 and 3 are then inserted in the expressions (62) and simplified to the following:

$$\begin{split} \delta M^{00\rho\sigma}h_{\rho\sigma} &= -\frac{1}{10}k^{(6)0m0m0n0}\nabla^{4}h_{00} + \{\frac{1}{12}s^{(4)0kl0kl} + \frac{1}{30}s^{(6)0kl0klmm}\nabla^{2} \\ &+ \frac{1}{30}k^{(6)0k0klmlm}\nabla^{2}\} \times (\partial_{i}\partial_{j} - \delta_{ij}\nabla^{2})h_{ij}, \end{split} \tag{63} \\ \delta M^{0i\rho\sigma}h_{\rho\sigma} &= \{\frac{1}{24}s^{(4)0kl0kl} + \frac{1}{60}s^{(6)0kl0klmm}\nabla^{2} - \frac{1}{30}k^{(6)0k0klmlm}\nabla^{2}\} \\ &\times (\delta^{ij}\nabla^{2} - \partial^{i}\partial^{j})h_{0j} - \frac{1}{24}(^{*}q_{0}^{0l0l})\epsilon^{ijk}\nabla^{2}\partial_{j}h_{0k}, \end{split} \tag{64} \\ \delta M^{ij\rho\sigma}h_{\rho\sigma} &= \{-\frac{1}{12}\left(s^{(4)0kl0kl} + \frac{1}{2}s^{(4)klmklm}\right) - \frac{1}{30}\left(s^{(6)0kl0klmm} + k^{(6)0k0klmlm}\right)\nabla^{2} - \frac{1}{72}s^{(6)klmklmnn}\nabla^{2} \\ &- \frac{1}{240}k^{(6)klklmnmn}\nabla^{2}\}\delta^{ij}\nabla^{2}h_{00} + \{\frac{1}{12}(s^{(4)0kl0kl} + s^{(4)klmklm}) + \frac{1}{30}(s^{(6)0kl0klmm} + k^{(6)0k0klmlm})\nabla^{2} + \frac{1}{36}s^{(6)klmklmnn}\nabla^{2} \\ &- \frac{1}{240}k^{(6)klklmnmn}\nabla^{2}\}\partial^{ij}h_{00} - \{\frac{1}{24}s^{(4)klmklm} + \frac{1}{12}s^{(6)klmklmn}\nabla^{2}\}\delta^{ij}\nabla^{2}h_{pp} \\ &+ \{\frac{1}{12}s^{(4)klmklm}\right) + \frac{1}{36}s^{(6)klmklmnn}\nabla^{2} - \frac{1}{60}k^{(6)klklmnmn}\nabla^{2}\}\nabla^{2}h^{ij} \\ &+ \frac{1}{80}k^{(6)klklmnmn}\nabla^{2}\partial^{ij}h_{pp} \\ &- \frac{1}{24}^{*}q_{0}^{lnln}(\epsilon^{mki}\partial_{m}\nabla^{2}h_{k}^{i} + \epsilon^{mkj}\partial_{m}\nabla^{2}h_{k}^{i}). \end{split} \tag{65}$$

When needed above, one uses the Kronecker delta δ^{ij} to raise spatial indices. Note that for the last of equations (65), one takes the trace in ij to obtain the result (28). The equations for the off-diagonal components $h_{ij} - \frac{1}{3}\delta_{ij}h_{kk}$ can be obtained from (65) by subtracting the trace appropriately. Like the sample case in section 3.1 (see equation (11)) $h_{ij} - \frac{1}{3}\delta_{ij}h_{kk}$ is sourced

Table 2. Mass dimension 4 and 5 coefficients expressed assuming isotropic coefficients only. The dual is defined by ${}^*q_{\lambda}^{\alpha\beta\gamma\delta} = -\frac{1}{3!}\epsilon_{\lambda\mu\nu\kappa}q^{\mu\nu\kappa\alpha\beta\gamma\delta}$ with $\epsilon_{0123} = +1$.

	3! 17	-1 0123
Coefficients	Tableau	isotropic form
$S^{(4)0ik0jl}$	$egin{bmatrix} i & j \ k & l \end{bmatrix}$	$\frac{1}{6}(\delta^{ij}\delta^{kl}-\delta^{kj}\delta^{il})s^{(4)0mn0mn}$
$s^{(4)0jlikm}$	$egin{bmatrix} i & j \ k & l \ m \end{bmatrix}$	0
$s^{(4)ikmjln}$	$egin{bmatrix} i & j \ k & l \ m & n \end{bmatrix}$	$\frac{1}{6}\epsilon^{ikm}\epsilon^{iln}s^{(4)pqrpqr}$
$q^{(5)0ij0k0l}$	$egin{bmatrix} i & k & l \ j \end{bmatrix}$	0
$q^{(5)0ik0ljm}$	$egin{array}{ c c c c c c c c c c c c c c c c c c c$	0
$q^{(5)ijk0l0m}$	$egin{bmatrix} i & l & m \ j \ k \end{bmatrix}$	$-rac{1}{3}\epsilon^{ijk}\delta^{lm}(^*q_0^{0n0n})$
$q^{(5)0jlimkn}$	$\begin{array}{ c c c c c }\hline j & i & k \\\hline l & m & n \\\hline \end{array}$	0
$q^{(5)ijl0mkn}$	$egin{bmatrix} i & k & m \ j & n \ \end{bmatrix}$	0
$q^{(5)ikmjnlp}$	$egin{array}{ c c c c c c c c c c c c c c c c c c c$	$-rac{1}{6}\epsilon^{ikm}(\delta^{jl}\delta^{np}-\delta^{jp}\delta^{nl})(^*q_0^{qrqr})$

by h_{00} and h_{jj} and since h_{00} is of primary interest in this work we do not include the solution here.

To compare the results with those obtained by looking at propagation effects in GWs, we record here the isotropic combination of coefficients in the gravity sector called $(k_I^{(6)})_{00}$. The spherical coefficients are defined by (see [99]),

$$\frac{1}{2}(\hat{s}^{+-+-} + \hat{k}^{++--}) = \sum_{jm} \omega^4 (-1)^j Y_{jm}(\hat{v}) (k_I^{(6)})_{jm}, \tag{66}$$

where the coefficients on the left hand side are to be evaluated at d=6 only, and from (5) with the substitution $\partial_{\mu} \rightarrow -ip_{\mu}$. The +, -, and the \hat{v} refer to a helicity basis for GW's so

Table 3. Mass dimension 6 coefficients expressed assuming isotropic coefficients only. For two of the sets of coefficients, $s^{(6)ikmjlnpq}$ and $k^{(6)imjnkplq}$, the expression in terms of Kronecker deltas is abbreviated due to its length. It can be calculated using the 'Young-Project' command of the *xTras* package for xTensor [104].

Coefficients	Tableau	Isotropic form
s ^{(6)0ik0jlmn}	$\begin{bmatrix} i & j & m \mid n \\ k & l \end{bmatrix}$	$\begin{array}{l} \frac{1}{60}(\delta^{in}\delta^{jm}\delta^{kl}+\delta^{im}\delta^{in}\delta^{kl}-\delta^{il}\delta^{jn}\delta^{km}-\delta^{il}\delta^{jm}\delta^{kn}\\ -\delta^{in}\delta^{jk}\delta^{lm}+\delta^{ij}\delta^{kn}\delta^{lm}-\delta^{im}\delta^{jk}\delta^{ln}+\delta^{ij}\delta^{km}\delta^{ln}\\ -2\delta^{il}\delta^{jk}\delta^{mn}+2\delta^{ij}\delta^{kl}\delta^{mn})s^{(6)0pq0pqrr} \end{array}$
s ⁽⁶⁾⁰ jlikmnp	$\begin{bmatrix} i & j & n & p \\ k & l \\ m \end{bmatrix}$	0
$s^{(6)ikmjlnpq}$	$egin{array}{ c c c c c c c c c c c c c c c c c c c$	$\frac{1}{90}(-\delta^{iq}\delta^{jp}\delta^{kn}\delta^{lm} - \delta^{ip}\delta^{jq}\delta^{kn}\delta^{lm} + \delta^{in}\delta^{jq}\delta^{kp}\delta^{lm} + \dots)s^{(6)}$
$k^{(6)0i0j0k0l}$	$egin{array}{ c c c c c c c c c c c c c c c c c c c$	$\frac{1}{15}(\delta^{ij}\delta^{kl}+\delta^{ik}\delta^{jl}+\delta^{il}\delta^{jk})k^{(6)0m0m0n0n}$
$k^{(6)0j0k0lim}$	$egin{bmatrix} i & l & j & k \ m \end{bmatrix}$	0
$k^{(6)0k0limjn}$	$\begin{bmatrix} i & j & k & l \\ m & n \end{bmatrix}$	$\begin{array}{l} \frac{1}{60}(-2\delta^{in}\delta^{im}\delta^{kl}-\delta^{in}\delta^{il}\delta^{km}-\delta^{il}\delta^{jm}\delta^{kn}-\delta^{in}\delta^{jk}\delta^{lm} \\ +\delta^{ij}\delta^{kn}\delta^{lm}-\delta^{ik}\delta^{jm}\delta^{ln}+\delta^{ij}\delta^{km}\delta^{ln}+\delta^{il}\delta^{jk}\delta^{mn} \\ +\delta^{ik}\delta^{jl}\delta^{mn}+2\delta^{ij}\delta^{kl}\delta^{mn})k^{(6)0p0pqrqr} \end{array}$
$k^{(6)0kil0mjn}$		$k^{(6)0kil0mjn} = k^{(6)0k0limjn} - k^{(6)0k0ilmjn}$
$k^{(6)0 lim jn kp}$	$ \begin{array}{c c c c} j & k & i & l \\ \hline n & p & m \end{array} $	0
$k^{(6)imjnkplq}$	$ \begin{array}{c c c} i & j & k & l \\ \hline m & n & p & q \end{array} $	$\frac{1}{240} (2\delta^{iq}\delta^{jp}\delta^{kn}\delta^{lm} + \delta^{ip}\delta^{jq}\delta^{kn}\delta^{lm} + \delta^{in}\delta^{jp}\delta^{kq}\delta^{lm} + \dots)k^{(6)rsrstutu}$

that $p_{\mu} = (-1, \hat{v})$. A plus or minus in an index indicates a contraction with the helicity basis vectors \mathbf{e}^+ and \mathbf{e}^- (see [77, 99] for more details). Focusing on only the isotropic piece $(k_I^{(6)})_{00}$ it can be shown the following relation holds:

$$(k_I^{(6)})_{00} = \sqrt{4\pi} \left[-\frac{1}{12} (s^{(6)0ij0ij00} + s^{(6)ijkijk00} + \frac{1}{5} s^{(6)0ij0ijkk} + \frac{1}{3} s^{(6)ijkijkll}) + \frac{1}{60} (4k^{(6)0i0i0j0j} + 8k^{(6)0i0ijkjk} + k^{(6)ijijklkl}) \right].$$
(67)

Large amplitude limit of the solution

Given the results of the section 3.2, we record here the large amplitude limit, where $\chi \sim -1/4$. Specifically we let $\chi = -1/4 + \epsilon$ and explore the solutions for small ϵ . When simplifying the

Table 4. Solutions for the Green function \mathcal{G}_1 from equation (42) in the (large amplitude) limit where $\chi = -1/4 + \epsilon$ for small ϵ . The sign choice for ϵ and the coefficient combination $k_2 + 2k_3$ are listed in the right two columns. Here, $\psi = |k_2 + k_3|/|k_2 + 2k_3|$ and the coefficient combinations k_1 , k_2 , and k_3 are defined in equation (29). Note that ψ and $R/|k_2 + 2k_3|$ must be of O(1) or smaller for the approximation to be valid. Error terms for these approximations are of order $\sqrt{\epsilon}$.

$\overline{\mathcal{G}_1}$	$\operatorname{sgn}(k_2+2k_3)$	$\operatorname{sgn}\epsilon$
$\frac{1}{2\pi R} \left[1 - \frac{1}{2} \exp\left(-\frac{R}{\sqrt{ k_2 + 2k_3 }}\right) \left[2 + \psi \frac{R}{\sqrt{ k_2 + 2k_3 }}\right] \right]$	+	+
$\frac{1}{2\pi R} \left[1 - \frac{1}{2} \exp\left(\frac{\pm iR}{\sqrt{ k_2 + 2k_3 }}\right) \left[2 \pm i\psi \frac{R}{\sqrt{ k_2 + 2k_3 }} \right] \right]$	-	+
$\frac{1}{2\pi R} - \frac{1}{2\pi R} \exp\left(-\frac{R}{\sqrt{ k_2 + 2k_3 }}\right) \left[\cos\left(2\psi\sqrt{\frac{ \epsilon }{ k_2 + 2k_3 }}R\right)\right]$	+	_
$+\frac{1}{4\sqrt{ \epsilon }}\sin\left(2\psi\sqrt{\frac{ \epsilon }{ k_2+2k_3 }}R\right)$		
$\frac{1}{2\pi R} - \frac{1}{2\pi R} \exp\left(-2\psi\sqrt{\frac{ \epsilon }{ k_2 + 2k_3 }}R\right) \left[\cos\left(\frac{R}{\sqrt{ k_2 + 2k_3 }}\right)\right]$	_	_
$+\frac{1}{4\sqrt{ \epsilon }}\sin\left(\frac{R}{\sqrt{ k_2+2k_3 }}\right)$		

solution (42) in this limit, the result depends on the sign of the coefficient combination $k_2 + 2k_3$ and the sign of ϵ . Thus the result breaks into four cases. Specifically, when expanding to the lowest order in ϵ we find the four solutions in the table 4.

Several features are clear in this limit. Firstly, as $\epsilon \to 0$, it can be shown that three of the four solutions in table 4 are finite. The fourth row, with $\mathrm{sgn}(k_2+2k_3)=-1$ and $\mathrm{sgn}\epsilon=-1$ diverges as $\epsilon \to 0$. Second, the solutions are oscillatory in R with no damping (second row -+ case), a mixture of damped and oscillatory behavior in R (third and fourth row +- and -- cases), or damped with no oscillations (first row ++ case). The nature of the solution depends critically on which part of the k_1 , k_2 , k_3 coefficient space one probes.

Special cases:
$$k_2^2 - k_1 k_3 = 0 \lor k_1 + 2k_2 = 0$$

We record here the solution for the Green function for the Newtonian potential when the coefficient combinations k_1 , k_2 , and k_3 (equation (29)) take on special values. When $k_2^2 - k_1 k_3 = 0$, we cannot apply the solution (42) directly. We go back to re-evaluate the Fourier transform integral (35) with the p^4 term absent. The result for G_1 , and G_2 , the Green functions for \bar{h}_{00} and \bar{h}_{jj} , are given by

$$G_{1}(\vec{r}, \vec{r}') = \frac{1}{\pi R} \left(1 - \frac{k_{1} + k_{2}}{k_{1} + 2k_{2}} e^{-i\frac{R}{\sqrt{k_{1} + 2k_{2}}}} \right),$$

$$G_{2}(\vec{r}, \vec{r}') = -\frac{1}{\pi R} \frac{k_{2} + k_{3}}{k_{1} + 2k_{2}} e^{-i\frac{R}{\sqrt{k_{1} + 2k_{2}}}}.$$
(68)

Note that when the sign of $k_1 + 2k_2$ is negative, the solution becomes a damped exponential of the Yukawa form. The Green function for h_{00} can be obtained from $G_1 = (1/2)(G_1 + G_2)$.

Also we consider here the special case when $k_2^2 - k_1 k_3 = 0$ and $k_1 + 2k_2 = 0$. In this case the nonstandard terms in the momentum space functions in (34) are constants, yielding delta functions with the Fourier transform. The Green function \mathcal{G}_1 is then given by

$$\mathcal{G}_1 = \frac{1}{2\pi R} + 2k_3 \delta^{(3)}(\vec{R}). \tag{69}$$

ORCID iDs

Quentin G Bailey https://orcid.org/0000-0001-5917-6850 Jennifer L James https://orcid.org/0000-0001-8940-8261

References

- [1] Lee J G, Adelberger E G, Cook T S, Fleischer S M and Heckel B R 2020 New test of the gravitational $1/r^2$ law at separations down to 52 μ m *Phys. Rev. Lett.* **124** 101101
- [2] Fujii Y 1971 Dilaton and possible non-Newtonian gravity Nat. Phys. Sci. 234 5–7
- [3] Donoghue J F 1995 Introduction to the effective field theory description of gravity Advanced School on Effective Theories (Almunecar, Granada, Spain) vol 26 pp 217–40
- [4] Arkani-Hamed N, Dimopoulos S and Dvali G R 1998 The Hierarchy problem and new dimensions at a millimeter Phys. Lett. B 429 263–72
- [5] Fischbach E and Talmadge C L 1998 The Search for Non-Newtonian Gravity (New York: Springer Science & Business Media)
- [6] Krause D E and Fischbach E 2001 Searching for extra dimensions and new string inspired forces in the Casimir regime Gyros, Clocks, Interferometers...: Testing Relativistic Gravity in Space (Lecture Notes in Physics) vol 562 pp 292–309
- [7] Murata J and Tanaka S 2015 A review of short-range gravity experiments in the LHC era Class. Quantum Grav. 32 033001
- [8] Adelberger E G, Heckel B R and Nelson A E 2003 Tests of the gravitational inverse square law Ann. Rev. Nucl. Part. Sci. 53 77–121
- [9] Kostelecký V A and Samuel S 1989 Spontaneous breaking of Lorentz symmetry in string theory Phys. Rev. D 39 683–5
- [10] Gambini R and Pullin J 1999 Nonstandard optics from quantum space-time Phys. Rev. D 59 124021
- [11] Carroll S M, Harvey J A, Kostelecký V A, Lane C D and Okamoto T 2001 Noncommutative field theory and lorentz violation *Phys. Rev. Lett.* 87 141601
- [12] Mattingly D 2005 Modern tests of Lorentz invariance Living Rev. Rel. 8 5
- [13] Tasson J D 2014 What do we know about Lorentz invariance? Rept. Prog. Phys. 77 062901
- [14] Addazi A et al 2022 Quantum gravity phenomenology at the dawn of the multi-messenger era—a review Prog. Part. Nucl. Phys. 125 103948
- [15] Mariz T, Nascimento J R and Yu Petrov A 2022 Lorentz symmetry breaking-classical and quantum aspects (arXiv:2205.02594)
- [16] Bailey Q G, Kostelecký A and Xu R 2015 Short-range gravity and Lorentz violation Phys. Rev. D 91 022006
- [17] Kostelecký V A and Mewes M 2017 Testing local Lorentz invariance with short-range gravity Phys. Lett. B 766 137–43
- [18] Weinberg S 2009 Effective field theory, past and future *Proc. Sci.* CD09 1
- [19] Kostelecky V A and Potting R 1995 CPT, strings and meson factories *Phys. Rev.* D 51 3923–35
- [20] Colladay D and Kostelecký V A 1997 CPT violation and the standard model Phys. Rev. D 55 6760-74
- [21] Colladay D and Kostelecký V A 1998 Lorentz-violating extension of the standard model *Phys. Rev.* D 58 116002
- [22] Kostelecký V A 2004 Gravity, Lorentz violation and the standard model *Phys. Rev.* D **69** 105009
- [23] Cornish N, Sampson L, Yunes N and Pretorius F 2011 Gravitational wave tests of general relativity with the parameterized Post-Einsteinian framework *Phys. Rev.* D 84 062003

- [24] Mirshekari S, Yunes N and Will C M 2012 Constraining Lorentz-violating modified dispersion relations with gravitational waves. Phys. Rev. D 85 024041
- [25] Will C M 2014 The confrontation between general relativity and experiment Living Rev. Rel. 17 4
- [26] Jacobson T and Mattingly D 2001 Gravity with a dynamical preferred frame *Phys. Rev.* D 64 024028
- [27] Alexander S and Yunes N 2009 Chern-Simons modified general relativity *Phys. Rept.* 480 1–55
- [28] Berti E et al 2015 Testing general relativity with present and future astrophysical observations Class. Quantum Grav. 32 243001
- [29] Okounkova M, Farr W M, Isi M and Stein L C 2022 Constraining gravitational wave amplitude birefringence and Chern-Simons gravity with GWTC-2 Phys. Rev. D 106 044067
- [30] Hehl F W, Von Der Heyde P, Kerlick G D and Nester J M 1976 General relativity with spin and torsion: foundations and prospects Rev. Mod. Phys. 48 393–416
- [31] Bluhm R 2015 Explicit versus spontaneous diffeomorphism breaking in gravity *Phys. Rev.* D 91 065034
- [32] Kostelecký V A and Li Z 2021 Backgrounds in gravitational effective field theory Phys. Rev. D 103 024059
- [33] Fischbach E, Haugan M P, Tadic D and Cheng H-Y 1985 Lorentz noninvariance and the Eotvos experiments Phys. Rev. D 32 154
- [34] Kostelecky V A and Tasson J 2009 Prospects for large relativity violations in matter-gravity couplings Phys. Rev. Lett. 102 010402
- [35] Kostelecky A V and Tasson J D 2011 Matter-gravity couplings and Lorentz violation Phys. Rev. D 83 016013
- [36] Pihan-Le Bars Hène et al 2019 New test of Lorentz invariance using the microscope space mission Phys. Rev. Lett. 123 231102
- [37] Podolsky B 1942 A generalized electrodynamics Part I-non-quantum Phys. Rev. 62 68–71
- [38] Pais A and Uhlenbeck G E 1950 On field theories with nonlocalized action *Phys. Rev.* 79 145–65
- [39] Woodard R P 2015 Ostrogradsky's theorem on Hamiltonian instability Scholarpedia 10 32243
- [40] Bailey Q G 2021 Construction of higher-order metric fluctuation terms in spacetime symmetrybreaking effective field theory Symmetry 13 834
- [41] Bonder Y and Peterson C 2020 Explicit Lorentz violation in a static and spherically-symmetric spacetime Phys. Rev. D 101 064056
- [42] O'Neal-Ault K, Bailey Q G and Nilsson N A 2021 3+1 formulation of the standard-model extension gravity sector *Phys. Rev.* D 103 044010
- [43] Reyes C M and Schreck M 2021 Hamiltonian formulation of an effective modified gravity with nondynamical background fields *Phys. Rev.* D 104 124042
- [44] Reyes C M and Schreck M 2022 Modified-gravity theories with nondynamical background fields Phys. Rev. D 106 044050
- [45] Kostelecký V A and Mewes M 2016 Testing local Lorentz invariance with gravitational waves Phys. Lett. B 757 510–4
- [46] Kostelecký V A and Mewes M 2018 Lorentz and diffeomorphism violations in linearized gravity Phys. Lett. B 779 136–42
- [47] Bailey Q G and Kostelecký V A 2006 Signals for Lorentz violation in post-Newtonian gravity Phys. Rev. D 74 045001
- [48] Hees A, Bailey Q G, Bourgoin A, Pihan-Le Bars Hène, Guerlin C and Le Poncin-Lafitte C 2016 Tests of Lorentz symmetry in the gravitational sector *Universe* 2 30
- [49] Bonder Y and Leon G 2017 Inflation as an amplifier: the case of Lorentz violation *Phys. Rev.* D 96 044036
- [50] Reyes C M, Schreck M and Soto A 2022 Cosmology in the presence of diffeomorphism-violating, nondynamical background fields *Phys. Rev.* D 106 023524
- [51] Nilsson N A 2022 Explicit spacetime-symmetry breaking and the dynamics of primordial fields vol 5 (https://doi.org/10.1103/PhysRevD.106.104036)
- [52] Bourgoin A, Hees A, Bouquillon S, Le Poncin-Lafitte C, Francou G and Angonin M C 2016 Testing Lorentz symmetry with lunar laser ranging *Phys. Rev. Lett.* 117 241301
- [53] Muller H, Chiow S-wey, Herrmann S, Chu S and Chung K-Y 2008 Atom interferometry tests of the isotropy of post-Newtonian gravity *Phys. Rev. Lett.* 100 031101
- [54] Shao L 2014 Tests of local Lorentz invariance violation of gravity in the standard model extension with pulsars *Phys. Rev. Lett.* 112 111103

- [55] Abbott B P et al 2017 Gravitational waves and gamma-rays from a binary neutron star merger: GW170817 and GRB 170817A Astrophys. J. 848 L13
- [56] Liu X, He V F, Mikulski T M, Palenova D, Williams C E, Creighton J and Tasson J D 2020 Measuring the speed of gravitational waves from the first and second observing run of Advanced LIGO and Advanced Virgo Phys. Rev. D 102 024028
- [57] Shao L 2020 Combined search for anisotropic birefringence in the gravitational-wave transient catalog GWTC-1 Phys. Rev. D 101 104019
- [58] Wang Z, Shao L and Liu C 2021 New limits on the Lorentz/CPT symmetry through 50 gravitational-wave events *Astrophys. J.* **921** 158
- [59] O'Neal-Ault K, Bailey Q G, Dumerchat T, Haegel L and Tasson J 2021 Analysis of birefringence and dispersion effects from spacetime-symmetry breaking in gravitational waves *Universe* 7 380
- [60] Kostelecký V A and Russell N 2011 Data tables for Lorentz and CPT violation Rev. Mod. Phys. 83 11–31
- [61] Bonder Y 2022 On the Hamiltonian of gravity theories whose action is linear in spacetime curvature 9th Meeting on CPT and Lorentz Symmetry
- [62] Kostelecky A 2011 Riemann-Finsler geometry and Lorentz-violating kinematics Phys. Lett. B 701 137–43
- [63] Lammerzahl C, Perlick V and Hasse W 2012 Observable effects in a class of spherically symmetric static Finsler spacetimes Phys. Rev. D 86 104042
- [64] Kostelecký V A, Russell N and Tso R 2012 Bipartite Riemann–Finsler geometry and Lorentz violation Phys. Lett. B 716 470–4
- [65] Schreck M 2015 Classical kinematics and Finsler structures for nonminimal Lorentz-violating fermions Eur. Phys. J. C 75 187
- [66] Bluhm R and Kostelecký V A 2005 Spontaneous Lorentz violation, nambu-goldstone modes and gravity Phys. Rev. D 71 065008
- [67] Bluhm R, Fung S-H and Kostelecký V A 2008 Spontaneous Lorentz and diffeomorphism violation, massive modes and gravity Phys. Rev. D 77 065020
- [68] Horava P 2009 Quantum gravity at a Lifshitz point Phys. Rev. D 79 084008
- [69] Kostelecky V A and Potting R 2009 Gravity from spontaneous Lorentz violation Phys. Rev. D 79 065018
- [70] Altschul B, Bailey Q G and Kostelecký V A 2010 Lorentz violation with an antisymmetric tensor Phys. Rev. D 81 065028
- [71] Seifert M D 2009 Vector models of gravitational Lorentz symmetry breaking Phys. Rev. D 79 124012
- [72] Bluhm R, Bossi H and Wen Y 2019 Gravity with explicit spacetime symmetry breaking and the Standard-Model Extension *Phys. Rev.* D 100 084022
- [73] Eling C and Jacobson T 2006 Black holes in Einstein-aether theory Class. Quant. Grav. 23 5643–60
 - Eling C and Jacobson T 2010 Class. Quant. Grav. 27 049802 (erratum)
- [74] Casana R, Cavalcante A, Poulis F P and Santos E B 2018 Exact Schwarzschild-like solution in a bumblebee gravity model *Phys. Rev.* D 97 104001
- [75] Xu R, Liang D and Shao L 2022 Static spherical vacuum solutions in the bumblebee gravity model (arXiv: 2209.02209)
- [76] Kostelecký V A and Li Z 2021 Searches for beyond-Riemann gravity Phys. Rev. D 104 044054
- [77] Kostelecký V A and Mewes M 2009 Electrodynamics with Lorentz-violating operators of arbitrary dimension Phys. Rev. D 80 015020
- [78] Kostelecky V A and Lane C D 1999 Constraints on Lorentz violation from clock comparison experiments Phys. Rev. D 60 116010
- [79] Kostelecky V A and Mewes M 2002 Signals for Lorentz violation in electrodynamics Phys. Rev. D 66 056005
- [80] Kostelecký V A and Vargas A J 2015 Lorentz and CPT tests with hydrogen, antihydrogen and related systems Phys. Rev. D 92 056002
- [81] Long J C and Kostelecký V A 2015 Search for Lorentz violation in short-range gravity Phys. Rev. D 91 092003
- [82] Shao C-G, Tan Y-J, Tan W-H, Yang S-Q, Luo J and Tobar M E 2015 Search for Lorentz invariance violation through tests of the gravitational inverse square law at short-ranges *Phys. Rev.* D 91 102007

- [83] Shao C-G, Chen Y-F, Tan Y-J, Luo J, Yang S-Q and Tobar M E 2016 Enhanced sensitivity to Lorentz invariance violations in short-range gravity experiments *Phys. Rev.* D 94 104061
- [84] Shao C-G, Chen Y-F, Tan Y-J, Yang S-Q, Luo J, Tobar M E, Long J C, Weisman E and Kostelecký V A 2019 Combined search for a Lorentz-violating force in short-range gravity varying as the inverse sixth power of distance *Phys. Rev. Lett.* 122 011102
- [85] Chen Y-F, Tan Y-J and Shao C-G 2017 Experimental design for testing local lorentz invariance violations in gravity Symmetry 9 219
- [86] Bobowski J S, Patel H and Faizal M 2022 Novel setup for detecting short-range anisotropic corrections to gravity (arXiv:2208.01645)
- [87] Decca R S, Lopez D, Chan H B, Fischbach E, Krause D E and Jamell C R 2005 Constraining new forces in the Casimir regime using the isoelectronic technique *Phys. Rev. Lett.* 94 240401
- [88] Bailey Q G and Havert D 2017 Velocity-dependent inverse cubic force and solar system gravity tests Phys. Rev. D 96 064035
- [89] Simon J Z 1990 Higher derivative Lagrangians, nonlocality, problems and solutions *Phys. Rev.* D 41 3720
- [90] Eliezer D A and Woodard R P 1989 The problem of nonlocality in string theory Nucl. Phys. B 325 389
- [91] Kostelecký V A and Potting R 2021 Lorentz symmetry in ghost-free massive gravity Phys. Rev. D 104 104046
- [92] Arfken G B and Weber H J 2005 Mathematical Methods for Physicists (Mathematical Methods for Physicists) 6th edn, ed G B Arfken and H J Weber (Boston: Elsevier)
- [93] Lindell I and Olyslager F 01 2001 Polynomial operators and green functions *Prog. Electromagn. Res.* 30 59–84
- [94] Poisson E and Will C M 2014 Gravity (Cambridge: Cambridge University Press)
- [95] Kostelecky V A and Lehnert R 2001 Stability, causality and Lorentz and CPT violation Phys. Rev. D 63 065008
- [96] Yang S-Q, Zhan B-F, Wang Q-L, Shao C-G, Tu L-C, Tan W-H and Luo J 2012 Test of the gravitational inverse square law at millimeter ranges Phys. Rev. Lett. 108 081101
- [97] Shao C-G et al 2016 Combined search for Lorentz violation in short-range gravity Phys. Rev. Lett. 117 071102
- [98] Long J C, Chan H W, Churnside A B, Gulbis E A, Varney M C M and Price J C 2003 Upper limits to submillimeter-range forces from extra space-time dimensions *Nature* 421 922–5
- [99] Mewes M 2019 Signals for Lorentz violation in gravitational waves *Phys. Rev.* D 99 104062
- [100] Bailey Q G and Kostelecky V A 2004 Lorentz-violating electrostatics and magnetostatics *Phys. Rev.* D 70 076006
- [101] Lichtenberg D B 1978 Unitary Symmetry and Elementary Particles (New York: Academic Press)
- [102] Hamermesh M 1962 *Group Theory and its Application to Physical Problems* vol 1989 (Mineola, NY: Dover Publications)
- [103] Altschul B 2006 Limits on Lorentz violation from synchrotron and inverse compton sources Phys. Rev. Lett. 96 201101
- [104] Nutma T 2014 xTras: a field-theory inspired xAct package for mathematica Comput. Phys. Commun. 185 1719–38